REPORT DOCUMENTATION PAGE

AFRL-SR-AR-TR-06-0074

1. REPORT DATE (DD-MM-YYYY) 20-02-2006	2. REPORT TYPE Final Report	3. DATES COVERED (From - To) 12/15/02 - 12/14/05

4. TITLE AND SUBTITLE	5a. CONTRACT NUMBER
(U) Statistical Interpretation of Scalar Time-Series Measurements in Turbulent Partially Premixed Flames	5b. GRANT NUMBER F49620-03-1-0026
	5c. PROGRAM ELEMENT NUMBER 61102F

6. AUTHOR(S)	5d. PROJECT NUMBER 2308
Normand M. Laurendeau, Galen B. King, and Michael W. Renfro	5e. TASK NUMBER BX
	5f. WORK UNIT NUMBER

7. PERFORMING ORGANIZATION NAME(S) AND ADDRESS(ES)	8. PERFORMING ORGANIZATION REPORT NUMBER
School of Mechanical Engineering Purdue University West Lafayette, IN 47907-1288 Department of Mechanical Engineering University of Connecticut Storrs, CT 06269-3139	

9. SPONSORING / MONITORING AGENCY NAME(S) AND ADDRESS(ES)	10. SPONSOR/MONITOR'S ACRONYM(S)
AFOSR/NA Dr. Julian Tishkoff 4015 Wilson Boulevard Room 713 Arlington, VA 22203-1954	11. SPONSOR/MONITOR'S REPORT NUMBER(S)

12. DISTRIBUTION / AVAILABILITY STATEMENT

Approved for public release; distribution is unlimited.

13. SUPPLEMENTARY NOTES

14. ABSTRACT

Systematic comparisons have been obtained between hydroxyl time series as measured by picosecond time-resolved laser-induced fluorescence (PITLIF) and as predicted by large-eddy simulations (LES) for turbulent non-premixed H_2/N_2 jet diffusion flames. The measured and predicted autocorrelation functions for OH were found to collapse to the same shape when normalized by their integral time-scales. However, the time-scales predicted by LES were systematically low by a factor of 2-3 as compared to the PITLIF measurements. Time series for hydroxyl and total number density were also obtained using (PITLIF) and laser Rayleigh scattering (LRS), respectively, in non-premixed and partially premixed turbulent $H_2/CH_4/N_2$-air flames having similar Rayleigh cross-sections for air and the exhaust gases. The measured PSDs for OH and number density were found to collapse to the same shape when normalized by their respective integral time-scales. The density to OH time-scale ratio was typically 2-4, with larger ratios prevailing nearer non-premixed conditions owing to thinner OH flamelets. Finally, a novel PITLIF methodology has been developed which is capable of simultaneous two-point, time-series measurements of OH concentrations in turbulent flames. Two-point time-series data obtained in a standard H_2 diffusion flame at Re = 10,000 have been used to compute space-time correlations, spatial autocorrelation functions, and integral length-scales. Preliminary two-point results are discussed with a focus on implications for future measurements in gas-turbine combustors and thrust augmentors.

15. SUBJECT TERMS

Turbulent Partially Premixed Flames, Time Series, Autocorrelation Functions, Picosecond Time-Resolved Laser-Induced Fluorescence

16. SECURITY CLASSIFICATION OF:			17. LIMITATION OF ABSTRACT	18. NUMBER OF PAGES	19a. NAME OF RESPONSIBLE PERSON Julian M. Tishkoff
a. REPORT Unclassified	b. ABSTRACT Unclassified	c. THIS PAGE Unclassified	UL	26	19b. TELEPHONE NUMBER (include area code) (703) 696-8478

Statistical Interpretation of Scalar Time-Series Measurements in Turbulent Partially Premixed Flames

Normand M. Laurendeau, Galen B. King, and Michael W. Renfro[*]
School of Mechanical Engineering, Purdue University
West Lafayette, IN 47907-1288
[*]Department of Mechanical Engineering, University of Connecticut
Storrs, CT 06269-3139

Abstract

Systematic comparisons have been obtained between hydroxyl time series as measured by pico-second time-resolved laser-induced fluorescence (PITLIF) and as predicted by large-eddy simula-tions (LES) for turbulent non-premixed H_2/N_2 jet diffusion flames. The measured and predicted autocorrelation functions for OH were found to collapse to the same shape when normalized by their integral time-scales. However, the time-scales predicted by LES were systematically low by a factor of 2-3 as compared to the PITLIF measurements. Time series for hydroxyl and total number density were also obtained using (PITLIF) and laser Rayleigh scattering (LRS), respec-tively, in non-premixed and partially premixed turbulent $H_2/CH_4/N_2$-air flames having similar Rayleigh cross-sections for air and the exhaust gases. The measured PSDs for OH and number density were found to collapse to the same shape when normalized by their respective integral time-scales. For the non-premixed flames, the time-scales for OH and number density at the ra-dial location of peak temperature were found to scale similarly with $Re^{-1.41}$. The density to OH time-scale ratio on the jet centerline was typically 2-4, with larger ratios prevailing nearer non-premixed conditions owing to thinner OH flamelets. Finally, a novel PITLIF methodology has been developed which is capable of simultaneous two-point, time-series measurements of OH concentrations in turbulent flames. The experimental setup has a spatial resolution of less than 250 µm and a temporal resolution of 1 µs, thus permitting spatially and temporally resolved measurements of fluctuations in most turbulent flows. Two-point time-series data obtained in a standard H_2 diffusion flame at Re = 10,000 have been used to compute space-time correlations, spatial autocorrelation functions, and integral length-scales. Preliminary two-point results are discussed with a focus on implications for future measurements in non-premixed and partially premixed turbulent jet flames, gas-turbine combustors and thrust augmentors.

1

20060323059

1. Research Objectives

Quantitative measurements of radical species concentrations in flames are required for an understanding of important interactions between fluid mixing and chemical reactions (Drake and Pitz, 1985). Advances in laser-based techniques have made non-perturbing measurements of such species concentrations possible in recent years. In particular, laser-induced fluorescence (LIF) possesses both the spatial and temporal resolution necessary for monitoring radical concentrations in reacting flows (Barlow and Carter, 1994). Unfortunately, LIF usually suffers from an inverse dependence on the local quenching rate coefficient. Although laser-saturated fluorescence (LSF) permits measurements of species concentrations without recourse to quenching calculations (Reisel *et al.*, 1997), the LSF technique requires large input energies which demand a laser repetition rate on the order of 10 Hz. This repetition rate can provide mean concentrations, rms concentrations and probability density functions (PDFs), but it is clearly too slow to resolve species fluctuations in turbulent flames. High repetition rate lasers, on the other hand, can be utilized for measuring turbulent species fluctuations, but the quenching rate coefficient must be obtained within sampling times on the order of the Kolmogorov time scale.

As a consequence of the above limitations for the usual LIF methods, the LIF protocol chosen for this research program utilizes a mode-locked laser that has the temporal resolution and irradiance necessary to provide direct time-series measurements, thus yielding autocorrelation functions as well as more traditional PDFs. The resulting optical technique, picosecond time-resolved laser-induced fluorescence (PITLIF), operates by monitoring the LIF signal using a novel four-bin integrated photon-counting procedure. Three sequential bins are used to rapidly resolve temporal decays so as to obtain fluorescence lifetimes at frequencies exceeding 10 kHz. The remaining bin integrates over the entire fluorescence lifetime so as to obtain the integrated fluorescence signal. The quenching data from the first three bins can ultimately be used to correct the integrated data from the remaining bin, thus producing a temporal record of fluctuations in concentration which is independent of the local quenching environment. From this temporal record, quantitative autocorrelation functions and power spectral densities (PSDs) can be determined corresponding to local concentrations in the flame. The resulting integral time-scales can then be used for validation of theoretical turbulence and combustion models.

Over the past three years, we have implemented PITLIF for measurements of OH time series and thus integral time-scales for a wide range of turbulent jet flames. From such data, suitable statistical information has been compiled for comparisons to predictions from large-eddy simulations (LES). We have also developed a laser Rayleigh scattering (LRS) technique capable of providing integral time-scales for total number density, which were then compared with those for hydroxyl in a series of non-premixed and partially premixed flames. In addition, we have developed a new version of PITLIF that permits simultaneous time series at two nearby points in turbulent reactive flows. To set the stage for discussion of our work during the last three years, we first review the theory and basic photon-counting instrumentation for PITLIF. In so doing, we demonstrate our novel capability to obtain both temporal and spatial statistics for the current investigation.

2. Background

2.1 Rate-Equation Analysis of Fluorescence Signal

The basic PITLIF procedure, which produces quenching-independent measurements of number density, can be understood by applying the radiative rate equations to a simple two-level model. We begin with a laser pulse that excites molecules from the ground level to an excited electronic level. All of the initial population is assumed to be in the ground level before excitation; moreover, the width of the laser pulse, Δt, is short compared to the quenching time. For sufficiently low laser power, the number density in the excited level immediately following the laser pulse, N_2° (cm^{-3}), is given by

$$N_2^\circ = N_1^\circ \bar{W}_{12} \Delta t, \qquad (1)$$

2

where N_1° is the initial number density of the species of interest and $\overline{W}_{12}$ is the average rate coefficient for stimulated absorption (s^{-1}), as computed from integration over the exact laser pulse shape. Following the laser pulse, the population of the excited level decays back to the ground level. In the absence of laser irradiation, absorption and stimulated emission can be neglected so that during this decay the number density of the excited level is given by

$$N_2(t) = N_1^\circ \overline{W}_{12} \Delta t \exp(-t/\tau_f), \qquad (2)$$

where τ_f is the excited-state (or fluorescence) lifetime (s). The excited-state lifetime is given in terms of the rate coefficient for spontaneous emission, A_{21}, and that for quenching, Q_{21}, by

$$\tau_f = (A_{21} + Q_{21})^{-1}. \qquad (3)$$

The temporal fluorescence signal depends linearly on both the number density in the excited level and the collection volume, V_c (cm^3). Hence, the temporally resolved fluorescence decay is given by

$$S(t) = \overline{W}_{12} \Delta t \, A_{21} V_c N_1^\circ \exp(-t/\tau_f), \qquad (4)$$

where $S(t)$ represents the output of the PITLIF instrument in photons/second. While temporal analysis of $S(t)$ yields the fluorescence lifetime, integration gives

$$S_F = \int_0^\infty S(t)dt = \overline{W}_{12} \Delta t \, A_{21} V_c \tau_f N_1^\circ, \qquad (5)$$

which corresponds to the integrated fluorescence signal. All of the terms in Eq. (5) can be determined through calibration except τ_n and N_1°. For our two-level system, the excited-state lifetime can be determined from the decay represented by Eq. (4). Equation (5) can then be used to determine the initial number density corrected for electronic quenching. For a multilevel system, the total number density can be obtained from N_1° by using the appropriate Boltzmann fraction. In either case, the integrated fluorescence signal is proportional to the concentration of target molecules in the flame.

2.2 Experimental Setup and Procedure

A diagram of the laser system, including the burner, is shown in Fig. 1. A Spectra-Physics Tsunami, regeneratively mode-locked, Ti:Sapphire laser is pumped by a 20-W, Spectra-Physics argon-ion, laser and provides a pulse repetition rate of 80 MHz. For OH measurements, the resulting IR beam, with a temporal pulse width of 2.0 ps, is frequency tripled in a CSK SuperTripler. The output beam is re-collimated by two UV lenses and focused by a 20-cm focal length, 5.0-cm diameter UV lens to form the probe volume above the burner assembly. For the tripled beam, the spatial resolution is $200 \times 200 \times 40 \ \mu m^3$ based on the beam di-

Figure 1. Experimental setup for single-point PITLIF

ameter (e^{-2}) and the width of the monochromator entrance slit for the detection system. The laser power is 24-40 mW which results in an average probe volume irradiance of ~2.5×10^7 mW/cm^2. The $R_1(11)$ transition of the (0,0) vibronic band (306.5 nm) of OH was chosen for excitation. This spectral region displays an approximately $\pm 5\%$ variation in Boltzmann fraction over the relevant temperature range of 1500-2500 K.
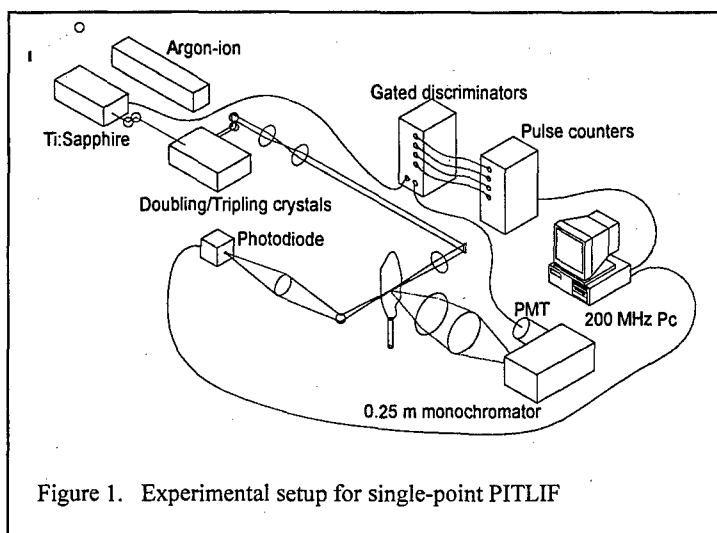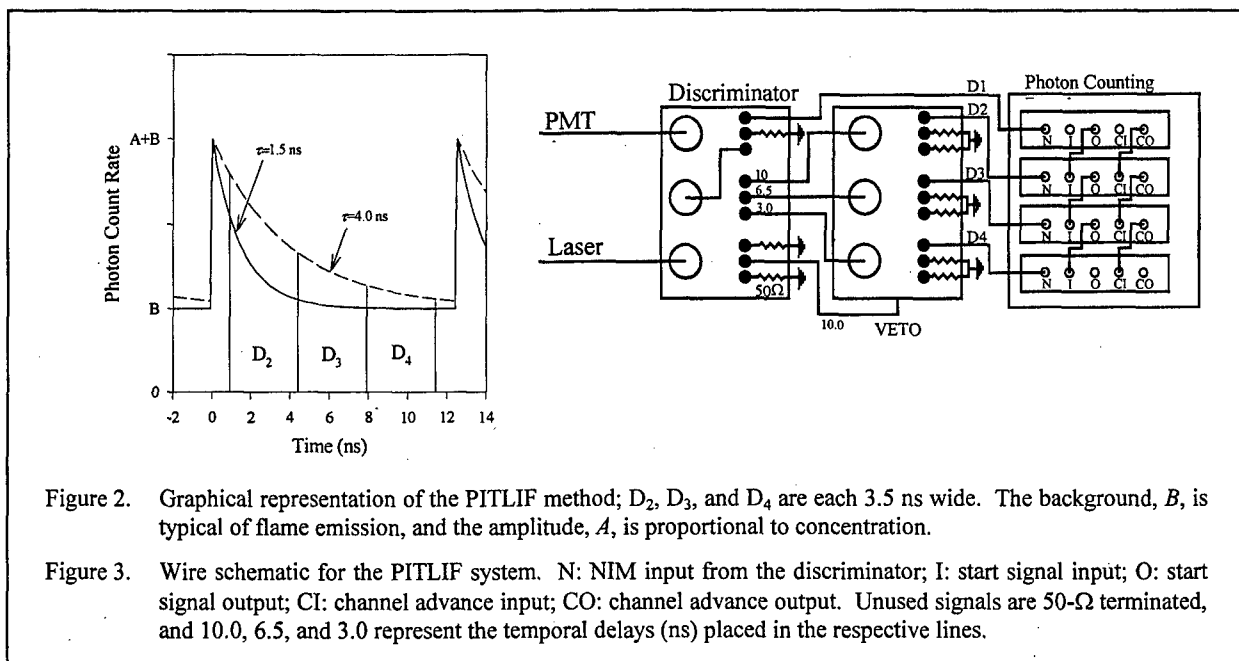
The OH fluorescence is collected at 90° from the incident laser beam by using two 14.1-cm focal-length, 5.1-cm diameter UV lenses. The wavelength of the measured fluorescence is selected by use of a 0.25-m monochromator. An adjustable slit at the entrance to the monochromator limits the probe volume along the beam path. For most measurements, the spectral window was adjusted to give a total bandwidth of 10 nm centered at 309 nm. A Hamamatsu HS5321 PMT detects the fluorescence at the exit plane of the monochromator. This PMT has a risetime of 700 ps and a transit time spread of 160 ps; by biasing at −2450 V, the single-photon pulse height was enhanced for subsequent leading-edge discrimination. Figure 2 shows representative fluorescence decays at fluorescence lifetimes (τ_f) of 1.5 and 4.0 ns, along with three areas, D_2, D_3 and D_4, specifying three of the four measurements for the gated, photon-counting system. The remaining measurement, D_1, which is not shown, is not gated and measures all photons; thus D_1 represents the total integrated fluorescence under either curve in Fig. 2.

Figure 2. Graphical representation of the PITLIF method; D_2, D_3, and D_4 are each 3.5 ns wide. The background, B, is typical of flame emission, and the amplitude, A, is proportional to concentration.

Figure 3. Wire schematic for the PITLIF system. N: NIM input from the discriminator; I: start signal input; O: start signal output; CI: channel advance input; CO: channel advance output. Unused signals are 50-Ω terminated, and 10.0, 6.5, and 3.0 represent the temporal delays (ns) placed in the respective lines.

A detailed wire schematic for the gated, photon-counting system is shown in Fig. 3. Briefly, the system consists of two LeCroy model 4608C, eight-channel discriminators connected to four EG&G Ortec logic-pulse counting boards. Several channels on the first discriminator are used to convert each PMT pulse into four logic (NIM) pulses. The second discriminator gates three of the four NIM pulses (D_2-D_4) from the first discriminator using a photodiode output from the Ti:Sapphire cavity. Separate cable delays for each of the three PMT inputs to the second discriminator ensure that each gate passes the appropriate portion of the fluorescence decay. The ungated NIM pulse from the first discriminator and the three outputs from the gated discriminator are separately counted by the four EG&G pulse counters shown schematically in Fig. 1. These comprise the measured bins D_2-D_4 of Fig. 2 and the integrated measurement D_1. The four photon-counting boards each have an 8192-channel memory and can be sampled simultaneously. Each channel acquires counts over many thousands of laser pulses as set in software. The maximum sampling rate (channel advance rate) for the boards is 500 kHz, well above that needed for turbulence studies.

The fluorescence lifetime, τ_f, and the flame-emission background, B, can be found from the gated counts using the expressions (Pack $et\ al.$, 1998)

$$\tau_f = \frac{\Delta t}{\ln[(D_2 - D_3)/(D_3 - D_4)]} \qquad (6)$$

$$B = \frac{D_2 C^2 - D_4}{\Delta t (C^2 - 1)}, \qquad (7)$$

where Δt is the width of each integrated bin (3.5 ns) and $C = \exp(-\Delta t / \tau_f)$. Based on Eq. (4), the concentration of the excited state immediately following the laser pulse is proportional to the amplitude of the exponential decay, A, shown in Fig. 2, and can be determined from

$$A = \frac{D_2 - D_4}{\exp(-t_o / \tau_f)(1 - C^2)(1 - C)\tau_f}, \qquad (8)$$

where t_o is the delay between the laser pulse and the start of bin D_2. This amplitude is also directly proportional to the concentration of the ground state, following Eq. (1), which in turn is directly proportional to the number density of the molecule of interest multiplied by a temperature-dependent Boltzmann fraction. Since the excitation wavelength can be chosen to experimentally minimize the variation of the Boltzmann fraction with temperature, A in Eq. (8) can usually be taken as proportional to this number density.

At sampling rates needed for turbulent flames, corrections owing to photon pulse-pileup are required for Eqs. (6-8). The requisite procedure was developed by Renfro et al. (1999a), and has been shown to provide reliable fluorescence decay amplitudes, lifetimes, and backgrounds at data collection rates up to 35 million photoelectrons per second. The correction procedure is based on the following scenario. Upon receiving an analog pulse which meets the threshold criterion, the discriminator begins to output a NIM pulse. However, if a second acceptable analog pulse arrives during the time required to complete the pulse output, the discriminator is unable to respond and the measured count rate can be lower than the actual incoming pulse rate. Fortunately, the output pulse rate is directly related to the input pulse rate; hence, a one-to-one relationship can be derived such that the measured output rate can be used to infer the actual input rate.

The resulting iterative procedure, termed "saturate-and-compare," is similar to convolute-and-compare routines that are commonly used to evaluate instrumentation response functions for accurate determinations of fluorescence lifetimes (Renfro et al., 1999a). The general procedure is as follows: (1) assume values for the decay parameters (τ_f, B, and A); (2) simulate a perfect decay; (3) saturate the decay based on the observed behavior of the PITLIF system; (4) compute the simulated bin counts, D_2-D_4; and (5) compare the simulated and measured counts, eventually converging to the correct decay parameters. While the full mathematical procedure is described by Renfro et al. (1999a), the general scheme is based on simply fitting measured photoelectron count rates to a saturated exponential array to represent the fluorescence decay.

3. Research Accomplishments

We have previously demonstrated that our photon-counting procedures for PITLIF can be used to monitor fluctuations in OH concentration on the time-scale of turbulence (Renfro et al., 1999a; Renfro et al., 2000a; Renfro et al., 2000b). During the last three years, we applied PITLIF to measurements of OH statistics in turbulent non-premixed and partially premixed flames (Renfro et al., 2002; Renfro et al., 2004; Raguraman et al., 2004). We also implemented a related technique to obtain similar time-series measurements of total number density in such flames (Raguraman et al., 2004; Raguraman, 2005). These measurements were obtained via laser-Rayleigh scattering (LRS), thus permitting for the first time comparisons of integral time-scale for hydroxyl and total number density. While making such measurements, we examined PITLIF statistics and LES simulations for OH in turbulent non-premixed flames. In addition, stochastic simulations based on the laminar flamelet concept were used to compare predicted and experimental time scales for both hydroxyl and total number density. More recently, we developed a two-point version of PITLIF that now permits for the first time determination of spatial as well as temporal statistics in turbulent flames (Zhang et al., 2005).

3.1 PITLIF Measurements and LES Simulations for Turbulent Non-premixed Flames

Comparisons between PITLIF measurements and LES predictions were pursued by examining OH fluctuations in non-premixed jet flames (Renfro et al., 2004). While mixture fraction would be a preferable scalar for validating predictions of time-scales, its measurement is much more difficult so that the associated time-scales are not generally available. Because OH exists only in high-temperature regions, OH fluctuations are dominated by large-scale flame motion (Renfro et al., 2000b). In particular, OH integral time-scales are insensitive to quantitative values of OH concentration yet very sensitive to the OH layer width and movement (Renfro et al., 2002). Therefore, OH time-series statistics in a nonpremixed flame are expected to be indicative of overall flame motion, while accompanying comparisons to LES predictions should be a useful mechanism for testing the capabilities of LES simulations.

Time-series measurements of OH were obtained in a turbulent $50\%H_2/50\%N_2$, Re = 10,000 jet diffusion flame (flame H3, described by Pfuderer et al., 1996). The chosen flame represents a standard benchmark case used in the Turbulent Non-premixed Flame Workshop and has been studied previously by Meier et al. (1996) using single-shot Raman scattering, by Pfuderer et al. (1996) using laser-doppler velocimetry, and by Neuber et al. (1998) using combined laser-induced fluorescence (LIF) and Raman scattering. These authors report mean values and standard deviations for temperature and major-species concentrations in this flame. Kempf et al. (2002) find reasonable agreement between LES results and statistical data for temperature, mixture fraction and velocity. The time-series measurements reported here further characterize this specific flame and complement the previous single-time data.

The burner was identical to that used by Pfuderer et al. (1996) and consisted of an 8-mm tube with a thinned rim at the exit. Coflowing air with an exit velocity of 0.2 m/s was provided with a contoured 140-mm nozzle. The burner could be translated in axial and radial directions to change the position of the measuring location. Radial profiles of time-averaged [OH] were obtained at x/D = 10, 20, 30, and 40 by using a sampling rate of 10 Hz and an averaging time of five seconds. At each height, time-series measurements were subsequently obtained by using a larger sampling rate of 12 kHz. Fifty time series with 4096 points each were collected at all measurement locations. Time-series measurements were also obtained at the burner centerline for an axial range of x/D = 20-40 with a step-size of x/D = 2. PSDs, autocorrelation functions, and integral time scales were computed in the same manner as reported by Renfro et al. (1999b, 2000b), including a correction for the measured contribution of shot noise. The integral time scale was computed by fitting an exponential curve to the autocorrelation function after correcting for shot noise. The statistics were averaged over the fifty available time series to reduce noise. The signal-to-background ratio (SBR) for these measurements was about five at peak [OH] locations when using an average laser power of 7-8 mW. This SBR is relatively high compared to previous measurements and is sufficient to resolve temporal statistics, such as the integral time-scale, to within 15%.
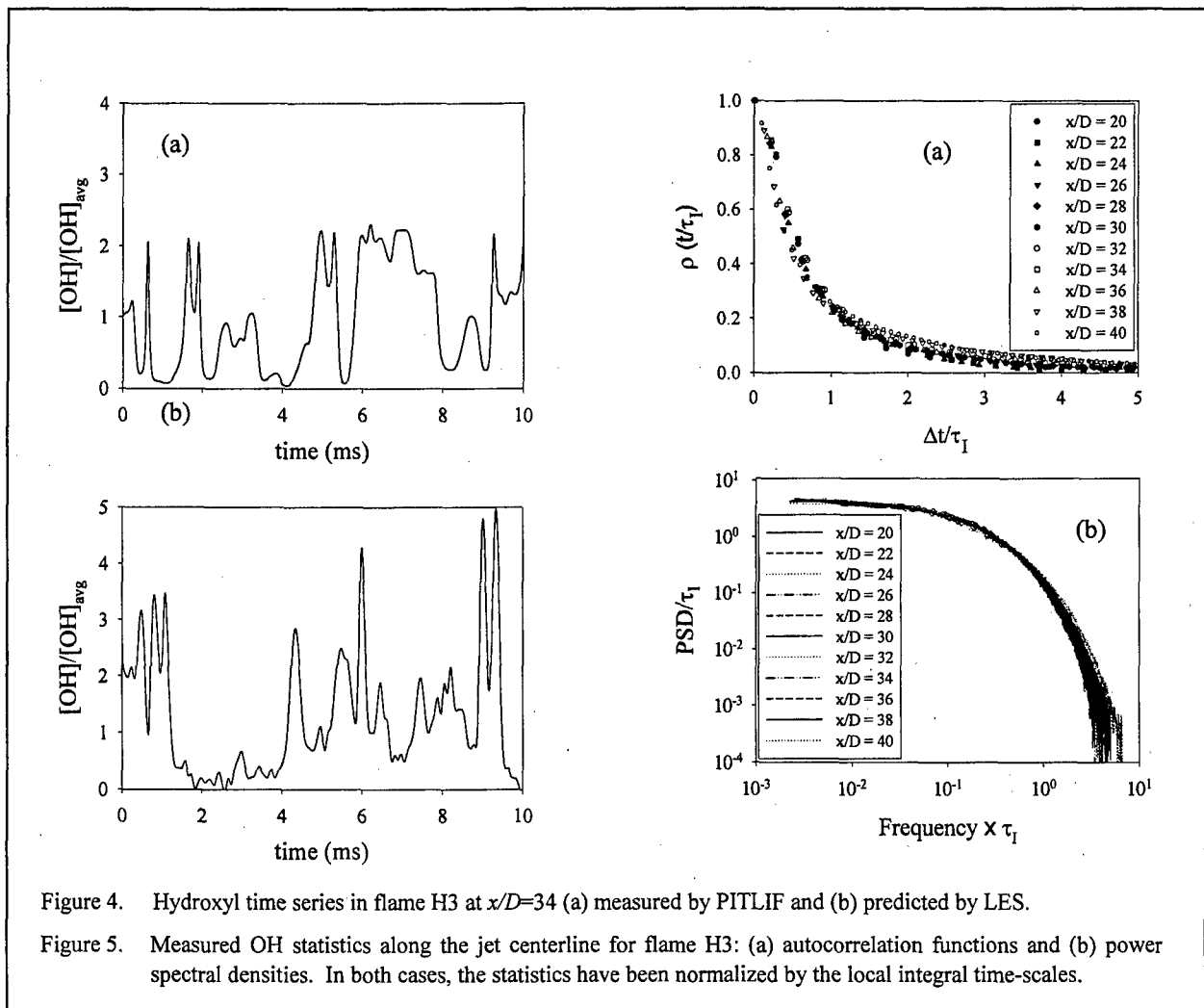
Numerical Methods

The large-eddy simulations were performed on a structured cylindrical grid with 60 radial, 32 circumferential and 256 axial staggered grid cells. For each simulation, 200,000 time steps were computed requiring approximately two weeks on a 2-GHz processor. The grid spanned 0.24 m in the radial direction and 0.40 m in the axial direction; the resulting spatial resolution was 2 mm in the axial direction. The solver utilized a second-order central scheme for convection and diffusion of momentum, and an explicit three-step Runge-Kutta scheme for time integration. A mixture-fraction approach was employed for all scalars. The scalar diffusion was computed using a second-order central scheme with a constant turbulent Schmidt number of 0.45. A total variation diminishing scheme was used for scalar convection, and a projection method was applied for pressure coupling. A turbulence model based on eddy viscosity was utilized for turbulent transport of momentum and scalars. In each cell, the chemical state was computed using a filtered mixture fraction and an assumed sub-grid, beta-PDF distribution. The PDF for the dissipation rate was described by a Dirac-delta function. Steady flamelet state relationships with equal species diffusivities were then applied to these PDFs. Given this approach, all scalar

quantities are ultimately functions of the favre-filtered mixture fraction, favre-filtered subgrid variance in mixture fraction, and favre-filtered scalar dissipation rate. Complete details of the LES model are available from Renfro *et al.* (2004) or Kempf *et al.* (2002).

The inlet conditions utilized either a turbulence inflow generator to provide structured temporal and spatial variations or steady boundary conditions with mean turbulent flow profiles but no turbulent structure. The 200,000 time steps for the H3 flame spanned a period of ~0.25 s. Time series for further analysis were extracted from the entire LES by ignoring initial offset periods. Simulated time series of filtered OH mass fraction and density were used point-by-point to create a time-series of OH mole fraction for direct comparison to the PITLIF measurements. The LES time series had step sizes of around 2 μs. The simulated OH time series were re-sampled at a fixed sampling rate of 100 kHz by linearly interpolating [OH] values every 10 μs. This even-step time series was then processed by utilizing the same numerical routines as used for the measured time series.

Results and Discussion

A representative time-series measurement on the jet centerline in flame H3, at $x/D = 34$ where the [OH] signal is at its maximum, is shown in Fig. 4(a). The trace represents the first 10 ms of data collected and visually demonstrates fluctuations in [OH] fluorescence as the hydroxyl layer oscillates with respect to the fixed laser beam. Figure 4(b) shows OH time series at the same location from LES. The measured and simulated time series are consistent with high levels of intermittency and similar structures

Figure 4.   Hydroxyl time series in flame H3 at x/D=34 (a) measured by PITLIF and (b) predicted by LES.

Figure 5.   Measured OH statistics along the jet centerline for flame H3: (a) autocorrelation functions and (b) power spectral densities. In both cases, the statistics have been normalized by the local integral time-scales.
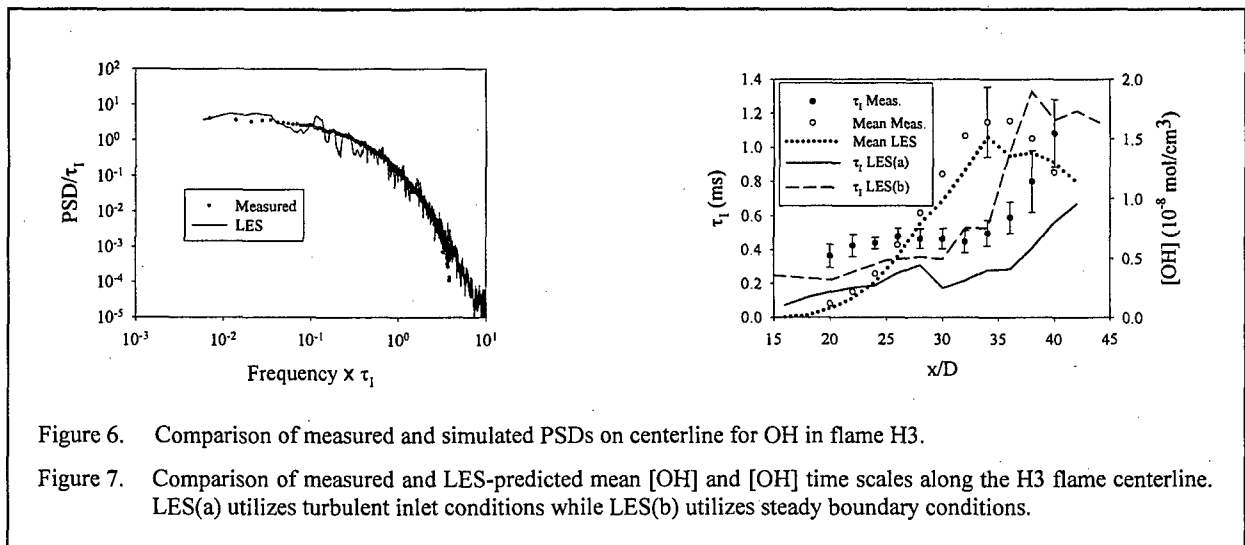
in the fluctuations. However, some differences are apparent, including the noise level in the two series. Figure 5(a) shows autocorrelation functions at the jet centerline for different axial locations in the range x/D = 20 to x/D = 40. Upon normalization via their respective integral time-scales, the autocorrelation functions display a very good collapse. This collapse is expected on the centerline, where the average velocities are high and the influence of the shear layer is less pronounced. The PSDs for these same locations are shown in Fig. 5(b), where the collapse to a single functional form is equally well observed.

Figure 6 shows a direct comparison of measured and simulated centerline PSDs for OH fluctuations at x/D = 30. Considerably more scatter occurs in the LES spectrum as the total usable time for the simulation is only 140 ms, compared to ~50 seconds of measured PITLIF data. The comparison displays excellent agreement, indicating that LES is predicting the correct distribution of large-scale fluctuations as determined by intermittent OH concentrations. At very high frequencies (not shown in Fig. 6), the LES spectrum displays slight departures from a single power-law decay. This change occurs above normalized frequencies of about 10 (10 times the inverse of the integral time-scale), which is the same order-of-magnitude as the flame velocity divided by the spatial resolution of LES. This departure probably results from limited spatial resolution in the simulations (~2 mm); fortunately, its magnitude and its presence has little influence on computed time scales as these are dictated by low-frequency fluctuations.

Figure 7 shows integral time-scales from both PITLIF and LES as a function of axial height along the H3 jet centerline. The errors bars were computed from standard deviations of over 10 separate measurements taken over a period of several months with two different flow systems and include both measurement and flame repeatability. The measured time scales, τ_I, range from 0.36 to 1.1 ms. The τ_I values are nearly constant below x/D = 34, which corresponds to the flame tip, but increase rapidly to significantly higher values farther downstream. Two predictions from large-eddy simulations are also shown in Fig. 7. LES(a) utilizes a turbulent inflow that provides fluctuating velocities at the jet exit while LES(b) utilizes a steady boundary condition with no fluctuations but with a correct mean velocity profile. The two simulations both generate axial profiles of [OH] integral time-scale that increase somewhat below the flame tip and rise rapidly beyond the tip; however, the predictions give significantly different quantitative values. The normalized PSDs for the two simulations are identical; hence, only quantitative values of the integral time-scale are apparently affected by the different boundary conditions. The simulated results using a turbulent boundary condition, which would be expected to be more realistic, are a factor of two smaller than the PITLIF measurements.

Based on these axial comparisons and also radial comparisons (Renfro et al., 2004), LES correctly predicts the shape of the PSD and thus the spectral distribution of scalar fluctuations, the shape of the axial and radial profiles for the integral time-scale, and the basic trends in τ_I between flames. However, quantitative predictions of the integral time-scale are typically a factor of two faster than measurements

Figure 6.   Comparison of measured and simulated PSDs on centerline for OH in flame H3.

Figure 7.   Comparison of measured and LES-predicted mean [OH] and [OH] time scales along the H3 flame centerline. LES(a) utilizes turbulent inlet conditions while LES(b) utilizes steady boundary conditions.

when using more realistic input conditions and are apparently strongly affected by the choice of boundary conditions. Other modeling assumptions or limitations in LES could also affect the prediction of scalar time-scales; fortunately, by varying pertinent parameters (Renfro et al., 2004), we find that most LES assumptions and limitations, including the spatial resolution, state-relationship and scalar dissipation-rate model, have only a secondary influence on the predicted OH integral time-scales. The dominant cause of discrepancies in OH predictions as compared to measurements arises from differences in the predicted integral time-scale for mixture fraction (Z). This time-scale for Z is affected throughout the flame by the inlet boundary conditions; thus, velocity time-scale measurements, especially at the burner exit, must be obtained in future work to assess the influence of assumed inlet conditions on quantitative time-scale predictions for typical jet flames.

In general, the integral time-scale for mixture fraction can be affected by both the spatial structure of the mixture-fraction field and the instantaneous velocities conditioned on mixture fraction. If spatial gradients in Z or if conditional velocities are over-predicted, then predicted time-scales will be reduced for typical scalars. Experimental data to validate mixture-fraction predictions in flame H3 are currently unavailable. However, Z-conditioned velocities have been partially addressed in jet flames by recent simultaneous measurements of flame structure and velocities by Han and Mungal (2000). In their nitrogen-diluted ethylene flames, the instantaneous CH layer was found to correspond to the so-called stoichiometric velocity, which is simply the bulk velocity multiplied by its stoichiometric mixture fraction. This result implies that the flame sheet is advected past any fixed probe volume with constant velocity below the flame tip.

Conclusions from Measurements and LES Simulations

Measurements of [OH] time series have been obtained in a standard turbulent H_2/N_2 jet diffusion flame. Large-eddy simulations for the same flame have been conducted, with time series for OH extracted at the same locations as for the PITLIF measurements. For both measurements and simulations, the PSDs collapse to a single curve when normalized by their respective integral time-scales. This self-similar PSD from LES compares well with that from measurements, even with changes to the LES grid resolution and boundary conditions. Therefore, LES correctly predicts the unique frequency distribution of scalar fluctuations. Relative changes in the integral time-scale are well predicted versus both axial and radial position, especially with turbulent boundary conditions. However, a quantitative comparison of integral time-scales shows that LES predictions are low by a factor of two when using realistic turbulent boundary conditions, and are close to the measurements when using steady boundary conditions.

Parametric changes to the LES model and its post-processing routines were used to examine the effect of transient start-up time, grid resolution, and sampling rate. In each case, the changes had a negligible effect on predicted integral time-scales. Post-processing of LES results indicated that the ratio of OH to mixture fraction time-scales is only weakly affected by reasonable variations in the OH state relationship or the LES-predicted rms profile for mixture fraction. Therefore, differences between measured and simulated OH time-scales and between temporal scales with alternate boundary conditions arise directly from changes in the predicted time-scale for mixture fraction. Incorrect predictions of Z time-scales impact any other predicted scalar, including temperature; thus, future work should focus on validation of time-scale predictions for mixture fraction. Correct predictions of Z time-scales would likely produce correct predictions of other scalars, such as OH, which are dominated by flamelet relationships. Validation of OH time-scales in these flames is equivalent to validating Z time-scales; however, the velocity time-scales at the burner exit must also be measured in future work to examine if LES can predict quantitative fluctuation rates when using more realistic boundary conditions.

3.2 PITLIF Measurements and Stochastic Simulations for Non-Premixed Flames

We have obtained time-series measurements of both hydroxyl and total number density for the first time in the same set of non-premixed turbulent jet flames using PITLIF and laser-Rayleigh scattering (LRS), respectively. In particular, [OH] and LRS measurements were obtained in a set of five non-

9

premixed flames in the range $13,100 \leq Re \leq 21,500$ using a fuel composed of $22.1\%CH_4$, $33.2\%H_2$ and $45.7\%N_2$. This particular fuel mixture was selected because its Rayleigh cross-section is essentially the same for the fuel as for the exhaust gases. Therefore, the resulting LRS measurements depend only on total number density and thus inversely on temperature. This particular fuel mixture has been extensively studied by Bergmann *et al.* (1998), Meier *et al.* (2000) and Schneider *et al.* (2003). Moreover, these same flames have been chosen as benchmarks for the Turbulent Non-premixed Flame (TNF) Workshops. Therefore, the time-series measurements reported in this study further characterize standard non-premixed flames and thus complement previous data for these standard flames.

The laser and detection system used for the OH measurements are identical to those employed by Renfro *et al.* (2000b). The system consists of a mode-locked laser and a photon-counting assembly that together record the LIF signal and fluorescence lifetime with a temporal resolution and bandwidth sufficient for time-series measurements. For the LRS measurements, a cw argon-ion laser was used at a nominal power of 22 W and a wavelength of 488 nm. The resulting LRS signal was amplified and then counted by utilizing a single ungated bin of the photon-counting system developed for the OH measurements. The spatial resolution for both [OH] and LRS was $200 \times 200 \times 40$ μm^3 based on the beam diameter and the width of the monochromator entrance slit used in the detection system. A fixed sampling rate of 16129 Hz was used for both the LRS and OH measurements. Signal-to-noise ratios were typically 2-3 for the OH measurements and 6-8 for the LRS measurements.

The burner for these flames was identical to that used by Bergmann *et al.* (19998) and consisted of an 8-mm diameter tube with a thinned rim at the exit. Co-flowing air with an exit velocity of 0.2 m/s was provided using a contoured 140-mm nozzle. The burner could be translated in both the axial and radial directions to change the position of the measured location. Fifty time series of 4096 points each were collected to obtain clean statistics. Autocorrelation functions, PSDs and integral time-scales were computed from these time series in the same manner as reported by Renfro *et al.* (2000b), including corrections, utilizing the measured PSDs, to eliminate contributions from shot noise (Renfro *et al.*, 2000a).
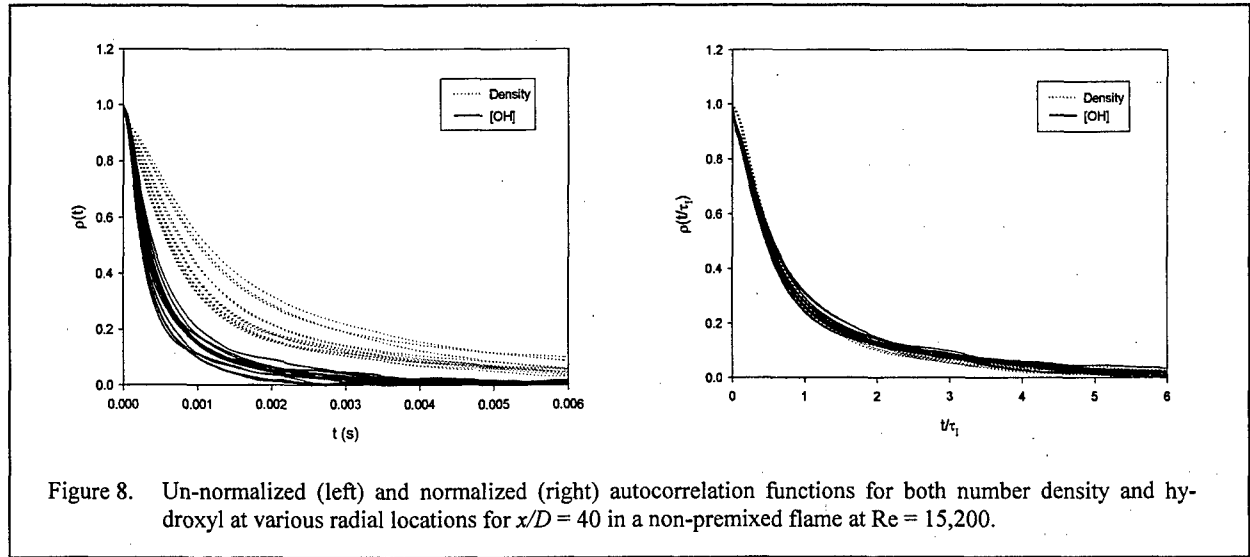

Figure 8.   Un-normalized (left) and normalized (right) autocorrelation functions for both number density and hydroxyl at various radial locations for $x/D = 40$ in a non-premixed flame at $Re = 15,200$.

Figure 8 shows autocorrelations functions at various radial locations for $x/D = 40$ within a single non-premixed flame at $Re = 15,200$. Both the original autocorrelation functions and those normalized by their respective integral time-scales are given for comparison. Integral time-scales, τ_I, were calculated by numerically integrating the autocorrelation functions over 100 data points. Figure 8 indicates that the normalized curves essentially collapse to a single autocorrelation function for both the LRS and [OH] measurements. This collapse implies that the relative distribution of fluctuation rates at a single point in the flow is the same as that at a different point for both fluctuations in OH and total number density.

Integral Time-Scales

The integral time-scale is a function of Reynolds number, jet diameter and flame location, as discussed by Renfro et al. (2000b). Since the PSDs and autocorrelation functions for a given flame are mostly self-similar when normalized by τ_I, the fluctuations in [OH] and number density throughout a particular flame can be fully described by their integral time-scale. Figure 9 displays time-scales for hydroxyl and total number density at axial locations along the jet centerline for five different Reynolds numbers. In general, the integral time-scales for both [OH] and number density rise with increasing distance from the nozzle, but drop with increasing Reynolds number (Renfro et al., 2000b). The integral time-scales for [OH] are generally 2-4 times lower than those for number density owing to increased scalar intermittency associated with enhanced fluctuations of the thinner OH layer.
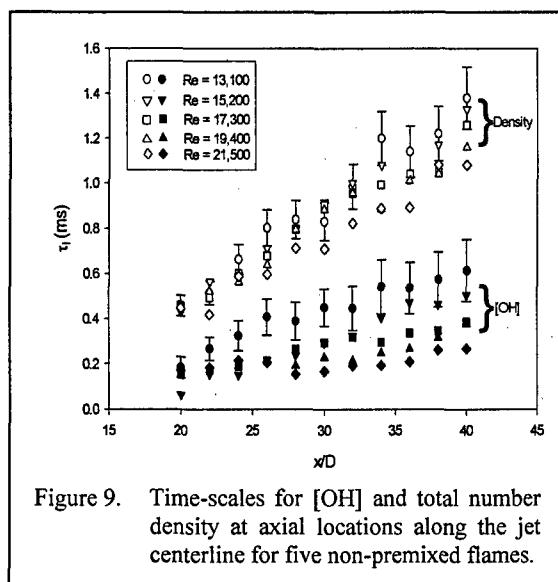
Figure 9. Time-scales for [OH] and total number density at axial locations along the jet centerline for five non-premixed flames.

Figure 10 shows the radial variation of integral time-scale for both hydroxyl and total number density based on measurements at x/D = 40 in the Re = 15,200 flame. Similar to trends along the jet centerline, the integral time-scales for [OH] and number density rise with increasing radial location. The [OH] time-scales are again 2-4 times lower than those for total number density. Generally, regions on the air side of the flame front are characterized by higher time-scales and thus by slower fluctuations owing to mixing of products with co-flow air. However, significantly less variation in integral time-scale occurs with radial location farther downstream. Figure 11 shows the ratio of number density to [OH] time-scales at various radial locations for x/D = 40 within the same Re = 15,200 flame. The mean [OH] radial profile is also shown for comparison to indicate the location of peak [OH]. The ratio of time-scales is highest at the jet centerline, decreases smoothly with increasing radial location towards the flame front, starts to rise in a rather haphazard manner slightly before the [OH] peak and continues to rise in that manner to the air side of the flame front.

In general, these results indicate that the ratio of density to [OH] time-scales invariably drops somewhat from the centerline to the flame front. This trend and the subsequent variation in time-scales near the flame front appear to result from the combined effects of heat release, molecular diffusion and
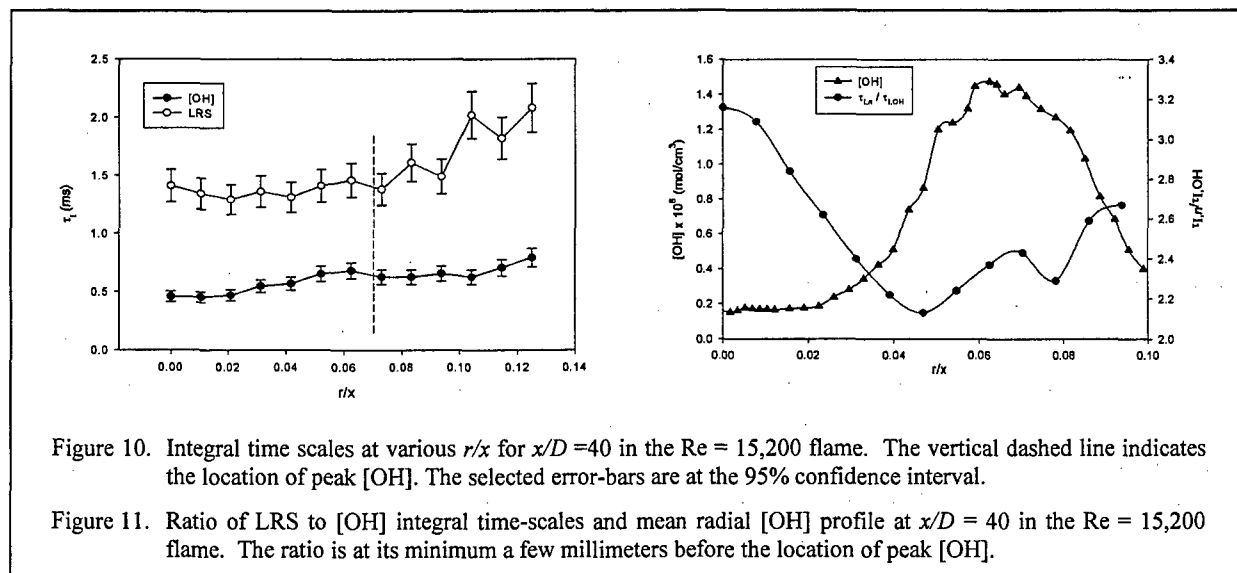
Figure 10. Integral time scales at various r/x for x/D =40 in the Re = 15,200 flame. The vertical dashed line indicates the location of peak [OH]. The selected error-bars are at the 95% confidence interval.

Figure 11. Ratio of LRS to [OH] integral time-scales and mean radial [OH] profile at x/D = 40 in the Re = 15,200 flame. The ratio is at its minimum a few millimeters before the location of peak [OH].

11

turbulent mixing. At lower axial heights, any time series for [OH] near the jet centerline represents fluctuations in hydroxyl molecules that have diffused from the flame front to the jet centerline. From a different perspective, the jet centerline is characterized by unburned fuel so that the local temperature is lower than that at the flame front. In addition, very little movement of the fuel core occurs, thus giving little variation in the resulting LRS signal. Consequently, at the jet centerline, the integral time-scale for total number tends to be higher than that for [OH] owing to a nearly complete absence of intermittency. In comparison, for positions nearer the flame front, the effect of heat release dominates and typically manifests itself through a radial broadening of the reaction zone. With increasing temperature, density fluctuations become more prominent and thus variations in the LRS signal become more discernable. Hence, relative to fluctuations in total number density, those for [OH] become less effective resulting in a drop in the ratio of density to [OH] time-scales with movement towards the flame front.

At the location of peak [OH], the mixture fraction is near its stoichiometric value. Considering the state relationship for mixture fraction, any appreciable variation in either [OH] or total number density away from the flame front arises from a change in mixture fraction. Consequently, near the mean [OH] peak, variations in number density should be proportional to those for [OH] irrespective of the Reynolds number. In other words, the strong influence of mixture fraction constitutes a possible explanation as to why time scales for number density and [OH] vary in a similar way with Re. Beyond the flame front and into the air side, the integral time-scales for number density are greater than those for [OH] because of slower mixing with co-flow air.

Renfro $et\ al.$ (2002) conducted time-series simulations using a laminar state-relationship for flames having a similar fuel-mixture composition and Reynolds number. Their simulations were able to predict uniquely the ratio of number density and [OH] time-scales to that presumed for mixture fraction. Both ratios, $\tau_{I,OH}/\tau_{I,Z}$ and $\tau_{I,n}/\tau_{I,Z}$, were found to be maximal at the jet centerline, reaching a minimum at the peak [OH] radial location, and then increasing again on the air side when plotted against suitably normalized coordinates. They attributed this reduction in time-scale ratio at the flame front to increased scalar intermittency. From this perspective, the variation of density to [OH] time-scales plotted in Fig. 11 is a new and interesting result that requires further investigation. In addition, a discernable rise apparently occurs in the fluctuation rate of [OH] near the jet centerline with increasing Re, as compared to that for number density, while the ratio of their fluctuation rates is nearly independent of Reynolds number near the flame front.

Statistical Analysis using a Stochastic Time-Series Model

The prediction of time-series behavior is of utmost interest to our research enterprise owing to its potential for validation of turbulent combustion models. A possible simplification for non-premixed flames, as suggested by analysis of scalar data, is that scalar fluctuations are mainly dominated by the convective motion of thin laminar flamelets. On this basis, knowledge of mixture-fraction fluctuations should be sufficient to predict fluctuation rates for other scalars in the flow. Renfro $et\ al.$ (2002) previously developed a stochastic time-series model to simulate such time series for the mixture fraction (Z). By building on this time-series model using a laminar state-relationship, we may obtain corresponding time series for hydroxyl and total number density. For the present simulations, we simply assume an invariant time-scale for the mixture fraction of 1 ms, based on the previous work of Renfro $et\ al.$ (2002).

The strategy for such simulations is to presume values for certain critical mixture-fraction statistics and to construct a realistic Z time series conforming to these statistics. The PDF and PSD were chosen as the important Z statistics since considerable information is available about their relative shapes. Using this approach, a synthetic Z time series will automatically have the correct frequency content and the correct range of instantaneous Z-values. On this basis, a simulated time series for mixture fraction was constructed using

$$Z(t_i) = \overline{Z} + \Im^{-1}\left\{\sqrt{\overline{Z'^2}\tau_{I,Z}PSD_Z(f_i\tau_{I,Z})} \times e^{i\Phi(f_i)}\right\}, \qquad (9)$$

where the mean and rms values for mixture fraction are taken from curve fits to the data of Meier *et al.* (2000) for identical flames, and the normalized PSD shape is computed via an exponential autocorrelation function (which is similar to the observed OH PSDs). The phase spectrum is generated randomly while the integral time-scale for mixture fraction, $\tau_{I,Z}$, is computed from the local velocity divided by the jet momentum half-width (Schneider *et al.*, 2000). On this basis, the integral time-scale can be taken as nearly invariant and equal to 1 ms.

The simulated time series for mixture fraction displays a near Gaussian PDF; hence, the time series from Eq. (9) can be mapped to the chosen PDF$_Z$. This map affects the shape of the PSD; thus, an iterative procedure was developed to simultaneously specify both the PDF and PSD shapes for Z. For comparison to OH data, the synthetic time series for Z were mapped by using a one-dimensional flamelet state-relationship, constructed using OPPDIF (Lutz *et al.*, 1996) with GRI-3.0 chemistry (Smith *et al.*, 1999). A similar procedure was used for the total number density. The resulting scalar time series could then be used to compute the mean, rms, PSD and τ_I for hydroxyl or total number density. Complete details of this simulation procedure are available from Renfro *et al.* (2002).

<u>Evaluation of Stochastic Predictions via Experimental Data</u>

By developing a realistic time series for mixture fraction, and then mapping it point-by-point using state-relationships, scalar time series may be obtained for hydroxyl and total number density. Figure 12 shows measured time series for [OH] and number density compared with predicted time series at the peak radial [OH] location for a standard Re = 15,200 flame at $x/D = 20$. The predicted Z time series are also given for comparison. While the measured and predicted time series cannot be expected to be identical, the obvious similarity in their structure is noticeable. The time series for number density display slower fluctuations while those for [OH] display more prominent on-off behavior owing to scalar intermittency. The scalar intermittency is a direct result of the narrowness of the state-relationship for [OH] as compared to that for number density. Whenever the mixture fraction approaches values beyond the limits of the [OH] state-relationship, the [OH] value goes to near zero. On the other hand, because the state-relationship for number density is wider, scalar intermittency is essentially absent in the time series for total number density.

From these predicted time series, we may compute statistics such as the autocorrelation function, PSD and integral time-scale. Figure 13, for example, shows measured and predicted autocorrelation functions for number density and hydroxyl at the peak radial [OH] location for $x/D = 20$ in a standard Re = 15,200 turbulent non-premixed flame. While our approximation of a constant Z time-scale of 1 ms is
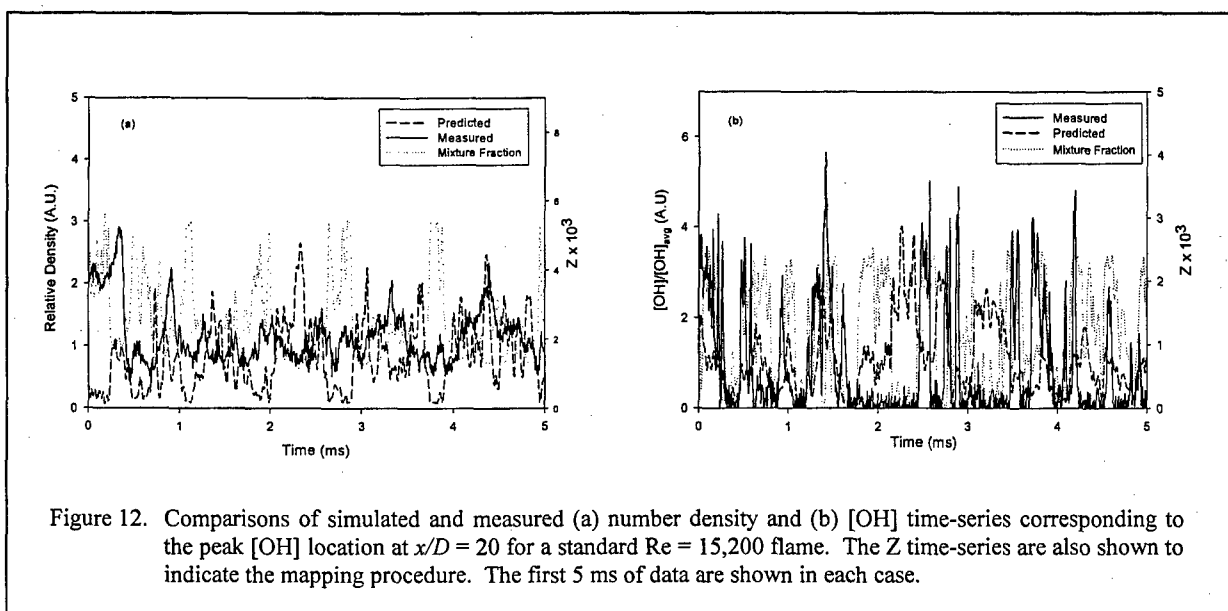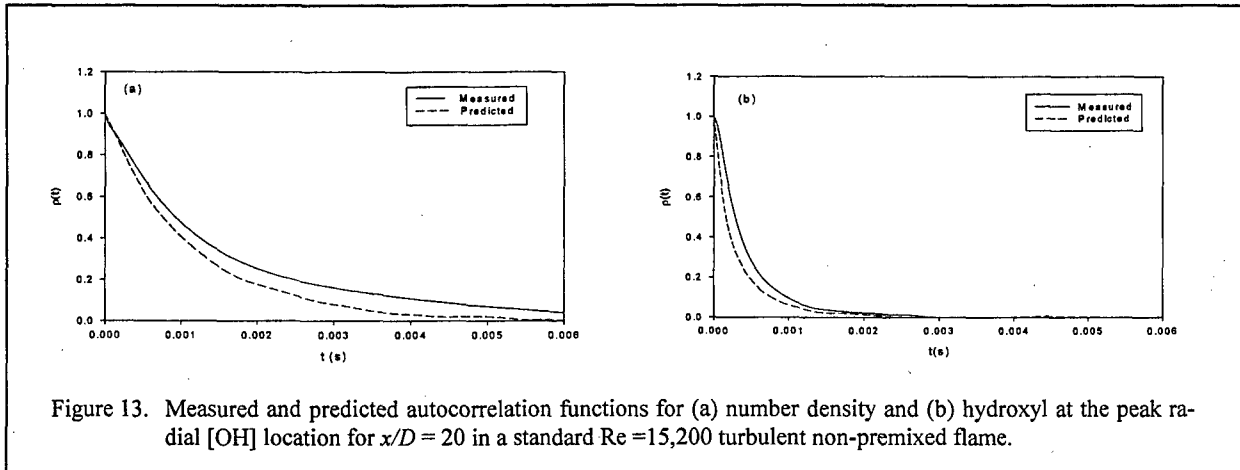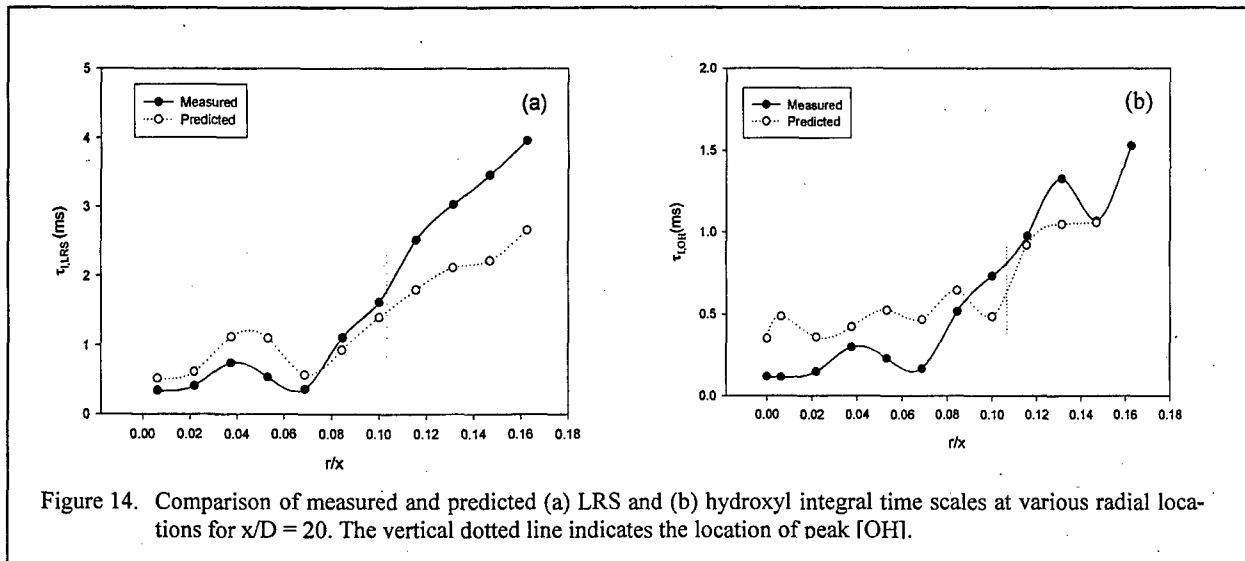

Figure 12. Comparisons of simulated and measured (a) number density and (b) [OH] time-series corresponding to the peak [OH] location at $x/D = 20$ for a standard Re = 15,200 flame. The Z time-series are also shown to indicate the mapping procedure. The first 5 ms of data are shown in each case.

certainly too simplistic, we nevertheless obtain remarkably good agreement between measured and predicted autocorrelation functions. In other words, the stochastic model correctly incorporates the influence of mixture fraction on fluctuations for both hydroxyl and total number density.

Figure 13. Measured and predicted autocorrelation functions for (a) number density and (b) hydroxyl at the peak radial [OH] location for $x/D = 20$ in a standard Re =15,200 turbulent non-premixed flame.

As shown in Fig. 14, excellent qualitative agreement exists between the measured integral-time scales and those predicted by the laminar-flamelet model. In particular, the predicted time-scales for number density and [OH] exhibit very similar trends to those obtained from the time-series measurements. Better quantitative agreement occurs near the location of peak [OH], which suggests less variation in the mean and rms of mixture fraction at the flame front for such non-premixed flames. At locations away from the flame front, the variation in mixture-fraction statistics could result in differences in predicted time-scale ratios. In general, however, the model correctly predicts the dip in integral time-scale before the flame front and its increase beyond the flame front. Considering the simplicity of the model and the rather bold assumption of an invariant Z time-scale of 1 ms, the agreement is actually quite fantastic!

Figure 14. Comparison of measured and predicted (a) LRS and (b) hydroxyl integral time scales at various radial locations for $x/D = 20$. The vertical dotted line indicates the location of peak [OH].

Renfro et al. (2002) found previously that predicted ratios of time-scales are very sensitive to input parameters such as the mean, variance and especially the integral time-scale for mixture fraction. Hence, a better choice of input conditions (especially time-scale) should result in better agreement between predictions and measurements. Future time-scale determinations for the mixture fraction in the same flame could provide critical input to further verify the predictive ability of the model. Nevertheless, the agree-

ment found between measured and predicted time-scales in these turbulent non-premixed flames certainly provides strong evidence for the forecasting ability of the laminar-flamelet model. It also confirms that turbulent non-premixed flames are indeed dominated by convective motion of thin reaction zones.

3.3 PITLIF Measurements for Partially Premixed Flames

Turbulent partially premixed flames are a pervasive feature of both gas-turbine combustors and thrust augmentors. However, such flames have previously not been studied via PITLIF, despite their practical significance and theoretical importance for understanding the statistical behavior of turbulent jets. We have recently shifted to partially premixed systems by investigating time series for hydroxyl and total number density, including their associated statistics, at various locations in a set of 18 $H_2/CH_4/N_2$-air jet flames at different fuel-side equivalence ratios and Reynolds numbers. Extensive work has previously been done by Bergmann *et al.* (1998) and Meier *et al.* (2000) on two non-premixed flames having Re = 15,200 and Re = 22,800 with the same fuel composition in an identical burner. The 18 flames investigated here provide an important extension to their work and form the basis for detailed modeling and experimentation in related partially premixed flames with the same fuel-mixture composition.

The fuel is a mixture of 22.1%CH_4, 33.2%H_2, and 44.7%N_2 in air. The Rayleigh cross-section for this mixture is again essentially constant and equal to that of air as well as combustion products. Hence, a change in fuel-side equivalence ratio has no effect on the Rayleigh scattering cross-section. This feature permits LRS measurements that are independent of cross-section and thus proportional to total number density. As before, the burner is basically a straight stainless tube with a thinned rim at the exit (Meier *et al.*, 1996). Co-flowing shop air is provided at an exit velocity of 0.2 m/s.

For each flame, time series were obtained at a fixed sampling rate of 16129 Hz, similar to that employed for the previous non-premixed flames. Fifty time series of 4096 points each were collected to obtain clean statistics at all measurement locations. Autocorrelation functions, power spectral densities (PSDs) and integral time-scales were computed from these time series in the same manner as reported by Renfro *et al.* (2000b), including corrections for contributions to shot noise. The peak signal-to-noise ratio (SNR) was about two for the [OH] measurements. For the number density data, the LRS signal to background flame emission was about 4-6.

Figure 15. LRS autocorrelation functions at various fuel-side equivalence ratios along the jet centerline at $x/D = 30$ for Re = 17,700.

Results for Partially Premixed Flames

Figure 15 shows LRS autocorrelation functions along the jet centerline for various fuel-side equivalence ratios at $x/D = 30$ and Re = 17,700. For a constant Reynolds number, the original autocorrelation functions are found to collapse to a single curve, but without normalization. This result clearly implies that fluctuations in total number density are dominated by the Reynolds number. Consequently, at any constant Re, we expect the integral time-scale for number density to display little variation with changes in fuel-side equivalence ratio. This conclusion is confirmed by Fig. 16(a), which displays similar time-scales for number density vs. axial location along the jet centerline, despite four different fuel-side equivalence ratios at Re = 17,700.

In comparison, we find, from Fig. 16(b), that the integral time-scale for [OH] is 2-4 times lower than that for total number density. This difference occurs primarily because of the intermittency observed in the [OH] time series. More importantly, at constant Re, the time-scale for [OH] varies considerably with changes in fuel-side equivalence ratio as compared to that for number density. In particular, the [OH] time-scale rises with decreasing fuel-side equivalence ratio, especially at higher Reynolds num-
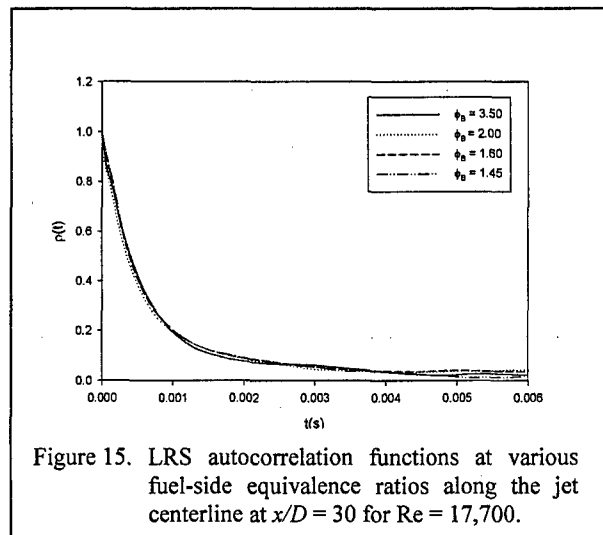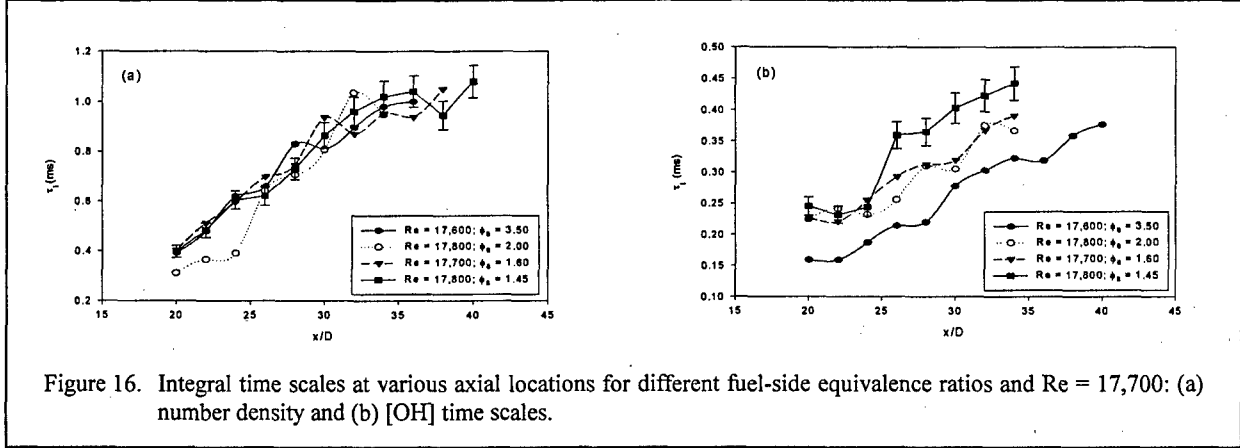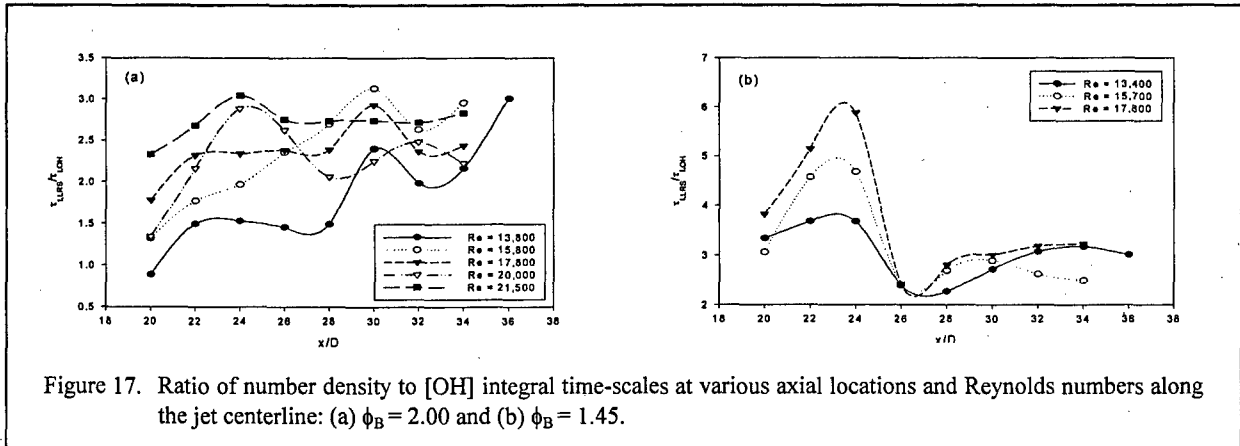
bers. Indeed, at lower fuel-side equivalence ratios, the [OH] time series is almost non-intermittent, similar to that for total number density. The resulting increase in average [OH] is invariably accompanied by less frequent bursts in [OH], which leads to greater integral time-scales. This enhancement in [OH] time-scale occurs again because of a radial broadening in the instantaneous reaction zone. In comparison, [OH] time series become progressively more intermittent at higher fuel-side equivalence ratios. Hence, the ratio of density to [OH] time-scales at higher fuel-side equivalence ratios often becomes greater than that associated with lower fuel-side equivalence ratios.

Figure 16. Integral time scales at various axial locations for different fuel-side equivalence ratios and Re = 17,700: (a) number density and (b) [OH] time scales.

The ratio of number density to [OH] time-scales for various Reynolds numbers at two constant fuel-side equivalence ratios is portrayed in Fig. 17. Similar to the behavior found previously for non-premixed flames, Fig. 17(a) verifies that an increase in Reynolds number enhances this time-scale ratio ($\phi_B = 2.00$). Furthermore, for non-premixed flames, we found that while this ratio rises with increasing Reynolds number, it is largely independent of axial height for a given Re. In contrast, for partially premixed flames, we find that while the ratio of density to [OH] time-scales rises with increasing Re, it also changes with axial height above the nozzle at higher fuel-side equivalence ratios.

Figure 17(b) shows the same time-scale ratio at various Reynolds numbers but at $\phi_B = 1.45$. Unlike Fig. 17(a), we notice that the profile shapes are very similar, even with changes in Reynolds number. In particular, the ratio increases substantially, drops to a minimum at about $x/D = 27$ and then rises again with increasing x/D. This is a very interesting result and suggests not only a coupling between density and [OH] fluctuations in low-equivalence ratio flames, but also a nearly constant ratio of time-scales near the flame tip. This behavior can be related to differences in flame height; in particular, the height of the $\phi_B = 1.45$ flame is lower than that of the $\phi_B = 2.0$ flame, with the tip of its flame brush very nearly at $x/D = 28$. This upper region represents a zone of almost constant temporal [OH] concentration, with minor

Figure 17. Ratio of number density to [OH] integral time-scales at various axial locations and Reynolds numbers along the jet centerline: (a) $\phi_B = 2.00$ and (b) $\phi_B = 1.45$.

16

changes in its associated time series. The similarity in time series for hydroxyl and total number density at $\phi_B = 1.45$ suggests that the time-scales should be related in a similar way. This interesting result requires further investigation, especially with respect to examining the effects of Reynolds number and fuel-side equivalence ratio on the ratio of integral time-scales.

Conclusions for Partially Premixed Flames

Autocorrelation functions for both hydroxyl and total number density more-or-less collapse to a single curve when normalized by their respective integral time-scales at constant Reynolds number and fuel-side equivalence ratio. On varying the equivalence ratio at constant Reynolds number, the [OH] autocorrelation functions show considerable variation in their rate of decay. The decay rate is higher as the fuel-side equivalence ratio rises, primarily because of an increase in [OH] intermittency. In comparison, the autocorrelation functions for number density merge to a single curve at constant Reynolds number, despite changes in fuel-side equivalence ratio. This behavior suggests that density fluctuations are primarily dominated by the Reynolds number. In fact, autocorrelation functions for partially premixed flames depend on Reynolds number in a manner similar to their non-premixed variants. Overall, the LRS autocorrelation functions exhibit a slower decay than the [OH] autocorrelation functions. This behavior results in higher time-scales for number density as compared to [OH].

Similar to the autocorrelation function, for a given Reynolds number and fuel-side equivalence ratio, the PSDs for hydroxyl and total number density at various axial locations along the jet centerline more-or-less collapse to a single curve when normalized by their respective integral time-scales. With increasing Reynolds number, the higher fluctuations observed in the [OH] time series are manifested in their PSDs as greater powers at higher frequencies. Furthermore, an increase in fuel-side equivalence ratio expresses itself in the [OH] PSDs by a similar extension to higher frequencies. This behavior results directly from a thinning of the reaction zone with rising fuel-side equivalence ratio, with a subsequent increase in [OH] intermittency. At constant Re, on the other hand, the PSDs for number density are unaffected by changes in fuel-side equivalence ratio, further confirming that density fluctuations are primarily dominated by the Reynolds number.

Integral time-scales for both number density and [OH] rise with increasing distance from the nozzle tip, but drop with an increase in Reynolds number at a given fuel-side equivalence ratio. The integral time-scales for number density are generally 2-4 times higher than those for [OH]. At constant Reynolds number, the time-scales for number density are mostly unaffected by changes in fuel-side equivalence ratio, further reinforcing our belief that such time-scales are primarily dominated by Re. In comparison, [OH] time-scales are found to depend strongly on both fuel-side equivalence ratio and Reynolds number. At lower fuel-side equivalence ratios, the density and [OH] fluctuations seem to be coupled, resulting in axial profiles for integral time-scale that are very similar. An increase in fuel-side equivalence ratio consistently reduces the [OH] time-scale. Moreover, an increase in Reynolds number enhances the rate of axial mixing in the flame core, thus further reducing the [OH] integral time-scale.

The ratio of number density to [OH] time-scales depends on both Reynolds number and axial height above the burner. This behavior is in contrast to that found for non-premixed flames, for which the ratio of integral time-scales for a given Re is largely invariant with axial height. At the lowest fuel-side equivalence ratio, the time-scale ratio higher in the flame is found to be largely invariant with Reynolds number. This feature is possibly related to a coupling between fluctuations in [OH] and number density as a result of non-intermittent time series for both [OH] and number density in these flames.

3.4 Two-Point PITLIF Technique for Turbulent Flames

We have recently developed a two-point version of PITLIF by optically defining two independent fluorescence channels along a single laser beam. This advanced PITLIF strategy can be used to obtain [OH] time series in turbulent non-premixed and partially premixed flames for comparison with previous single-point measurements in the same flames (Raguraman, 2005). More importantly, these time series can be analyzed in tandem to determine spatial autocorrelation functions and thus integral length scales.

17

A significant feature of the measurements is assessing calculated cross-correlations as influenced by both Reynolds number and specific location within the flame. We have previously demonstrated through single-point PITLIF the retrieval of temporal autocorrelation functions; in comparison, spatial information is most commonly recovered via PLIF imaging. However, the new two-point version of PITLIF permits cross-correlation measurements that include both spatial and temporal information. Such information is particularly important with respect to turbulence models that rely on Taylor's hypothesis for relating temporal and spatial gradients.

Development of Two-Point PITLIF

A two-point version of PITLIF that monitors two independent probe volumes along a single laser beam has been implemented by incorporating an additional PMT and detection setup in the previous single-point system. Given two closely-lying measurement locations, a single lens system can be used with the signal split prior to two separate detectors. Moreover, as previous work has shown that the fluorescence lifetime is irrelevant when determining quantitative time-scales, only two pulse counters are needed for each channel of the two-point PITLIF setup. These two photon-counting systems permit separate measurements of the combined fluorescence and chemiluminescence background from each PMT, but neglect variations in the fluorescence lifetime. The insignificance of lifetime fluctuations can be verified at each point by using our previous one-point PITLIF approach. Additional pulse counters could eventually be installed as part of the present data-taking system if lifetime variations are found to be significant.

The major difference between the present two-point version and that employed for previous single-point measurements (Renfro et al., 2000b) lies in the detection optics and photon-counting system. The basic idea behind the two-point configuration is to simultaneously collect fluorescence from two points in space through two different photomultiplier tubes (PMTs) and gate them separately using our previous photon-counting system (Pack et al., 1998). As shown in Fig. 18, fluorescence from the two probe volumes is collected at right angles to the laser beam by a 140-mm focal-length lens (L1), split by a beam splitter (BS) after passing through both an aperture stop (AS) and condensing lens (L2), and then refocused by two 150-mm focal-length lenses (L3 and L4) onto a corresponding monochromators and PMTs mounted on translation stages. Thus, PMT1 receives photons from the first probe volume and PMT2 receives photons from the second probe volume. The dimensions of each probe volume are $100 \times 100 \times 240 \mu m^3$, as defined by the laser-beam diameter and the width of the monochromator entrance slit. The second probe volume is moved relative to the first probe volume by translating PMT2 while keeping PMT1 stationary.

To demonstrate the efficacy of this new two-point strategy, [OH] time series were obtained in a standard non-premixed jet flame having a volumetric fuel composition of 50%H_2 and 50%N_2 (flame H3). The burner was identical to that used by Pfuderer et al. (1996) and consisted of an 8-mm tube with a thinned rim at the exit. The burner could be translated both in the axial and radial directions to change the measured position. Two-point OH measurements were taken at four peak [OH] locations corresponding to x/D = 10, 20, 30 and 35 at a fixed sampling rate of 12,048 Hz, where the position at x/D = 35 identifies the flame tip. Time series at a number of separation distances between the measured probe volumes were investigated, including the best matching point.
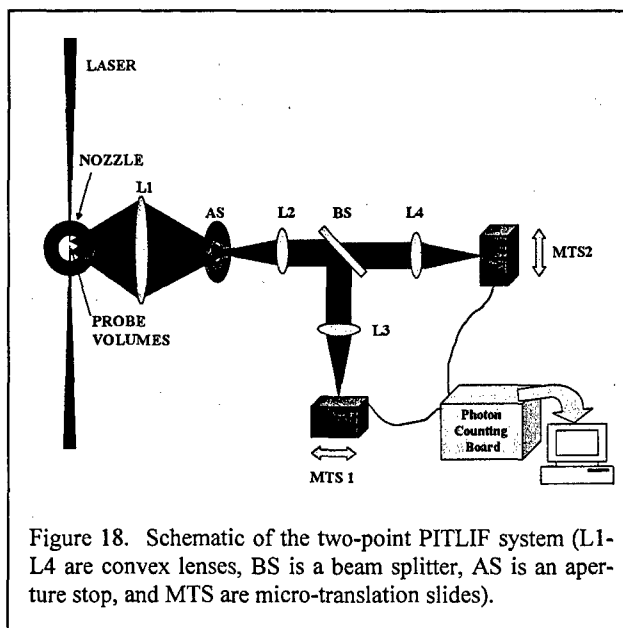

Figure 18. Schematic of the two-point PITLIF system (L1-L4 are convex lenses, BS is a beam splitter, AS is an aperture stop, and MTS are micro-translation slides).

The spatial resolution of the system is defined as the discernible minimum distance that the probe volume can be moved along the laser beam. We expect that two overlapping probe volumes will not give appreciably different simultaneous time series. Hence, the spatial resolution can be regarded as the lateral dimension of the probe volume, which is determined from the entrance slit of the monochromator divided by the magnification ratio of the detection optics. The magnification ratio was 2.1 and the entrance slit was set at 500 µm, which provides a spatial resolution of 240 µm along the laser beam direction. Decreasing the slit width may improve the spatial resolution; however, too small a slit size reduces the number of photons received such that the detected signal may be dominated by shot noise.

To resolve the finest structures of the scalar field, the measurement system requires a spatial resolution of the order of the Batchelor scale, λ_B, i.e., the scale at which molecular diffusion smoothes the scalar field. Following Wang et al. (2004), with velocity data taken from Dreizler (2001), we found that, for flame H3, most positions where measurements were taken have a Batchelor scale well above 200 µm. This result indicates that the hydroxyl field can be spatially resolved by our measurement system.

Figure 19 shows a representative two-point time-series measurement in flame H3 for various separation distances at the peak radial [OH] location and $x/D = 10$. The traces represent the first 20 ms of data collected and demonstrate fluctuations in fluorescence signal as the hydroxyl layer wavers with respect to the fixed laser beam. Since the hydroxyl layer is quite thin, the measured time series are very sensitive to movement of the probe volume. When the probe volumes of the two detectors overlap, as shown in Fig. 19(a), the simultaneous time series are almost identical, with minor differences likely due to system and background noise. This temporal overlapping of the time series decays as the separation distance increases beyond the minimum resolvable spatial length, as exhibited by Figs. 19(b) and 19(c). These results suggest that one way of testing the alignment of the detection optics is to compare cross-correlation functions between the two time series, which is actually routinely employed during experiments to normalize the separation distances.

Two-Point Statistics for Turbulent Flames

For simultaneous time series, a number of two-point statistics can be studied, including the space-time correlation, spatial autocorrelation function, integral length-scale and various cross spectra. The space-time correlation is defined as (Landahl and Mollo-Christensen, 1994)

$$f_{st}(r,\tau) = \frac{\left\langle OH'(x,t)OH'(x+r,t+\tau)\right\rangle}{\left[\left\langle OH'(x,t)^2\right\rangle\left\langle OH'(x+r,t)^2\right\rangle\right]^{1/2}}, \quad (10)$$

Figure 19. Representative two-point [OH] time series at x/D=10. The two PMTs are (a) at the same position or differ by (b) 1 mm and (b) 2.5 mm.

where $OH'(x,t)$ is the fluctuating component of the hydroxyl concentration, while r and τ are the displacement of the two probe volumes and the time delay, respectively (Zhang et al., 2005). They show, as expected, smooth transitions from a strongly correlated signal at similar space-time coordinates to weak correlations as either the time or the space coordinates becomes displaced relative to each other.
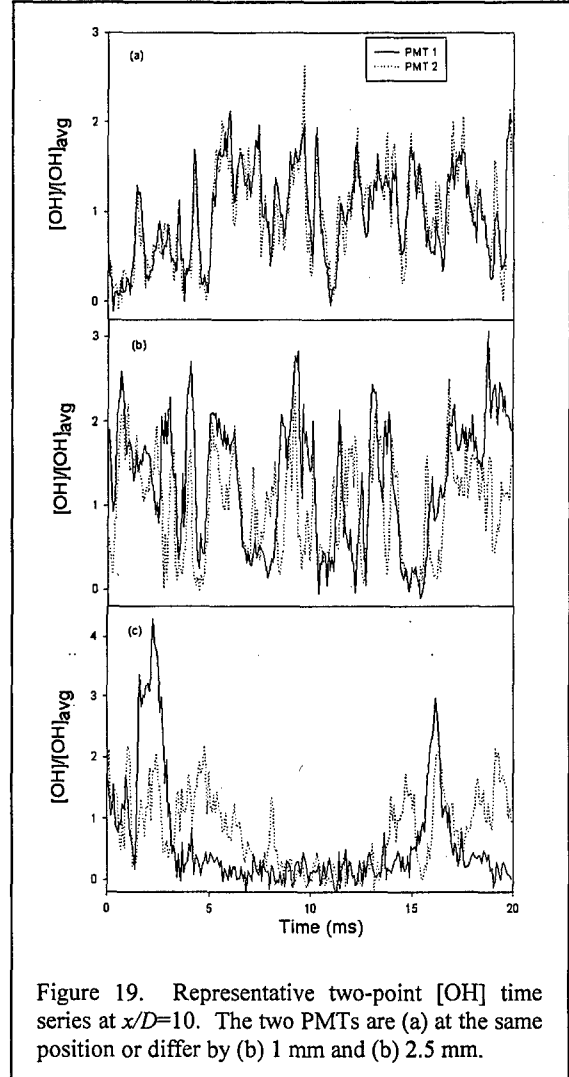
19

The spatial autocorrelation function is related to the space-time correlation by (Landahl and Mollo-Christensen, 1994)

$$f(r) = \frac{\left\langle OH'(x,t)OH'(x+r,t)\right\rangle}{\left[\left\langle OH'(x,t)^2\right\rangle\left\langle OH'(x+r,t)^2\right\rangle\right]^{1/2}} = f_{st}(r,\tau=0),$$
(11)

from which the integral length-scale can be defined as
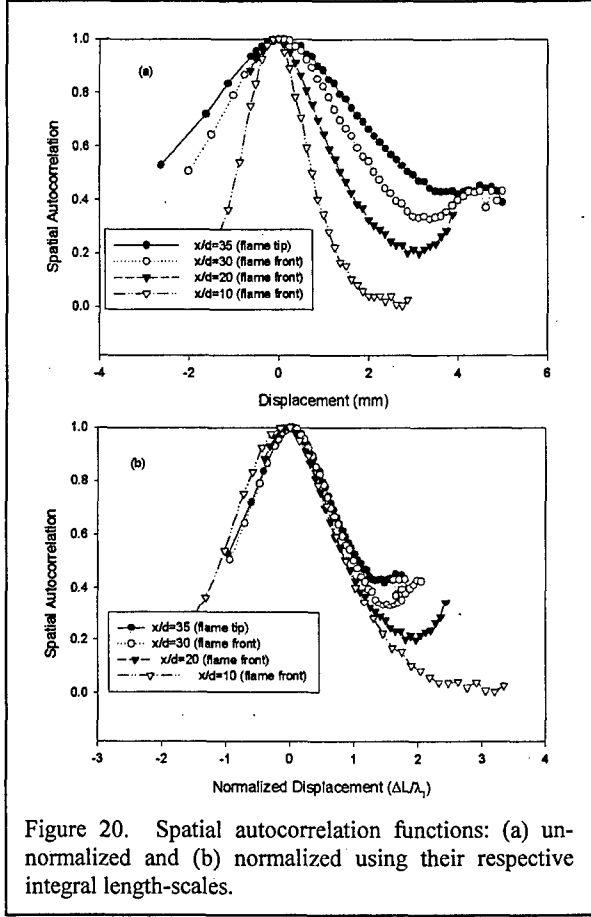
$$\lambda_l = \int f(r)dr.$$
(12)

Figure 20. Spatial autocorrelation functions: (a) un-normalized and (b) normalized using their respective integral length-scales.
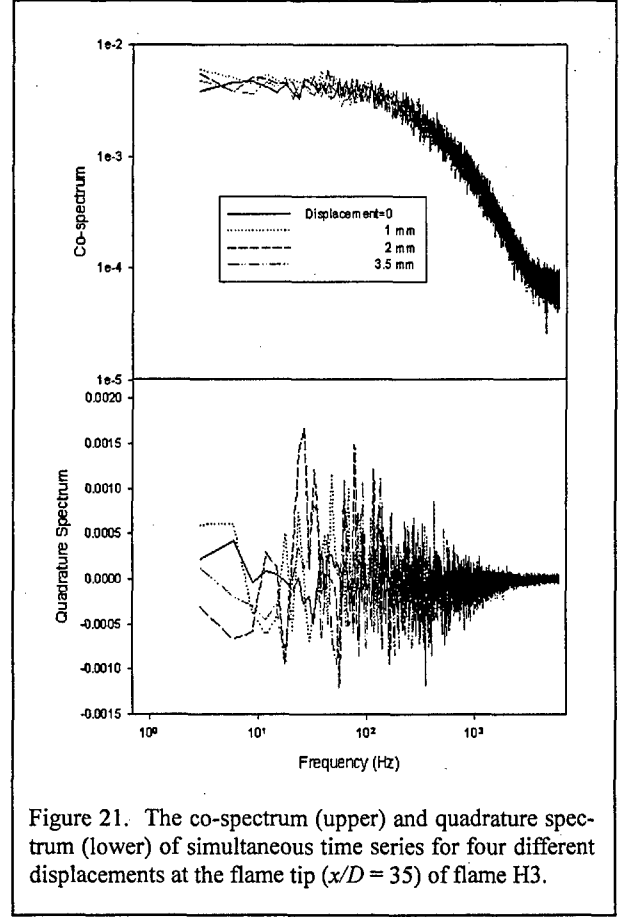
Figure 21. The co-spectrum (upper) and quadrature spectrum (lower) of simultaneous time series for four different displacements at the flame tip ($x/D = 35$) of flame H3.

Spatial autocorrelation functions are plotted in Fig. 20(a). We find that $f(r)$ at $x/D = 30$ displays the widest waist while that at $x/D = 10$ has the narrowest, which comports with the thick OH region high in the flame and the thinner OH layer in the shear layer lower in the flame. As for the temporal autocorrelation function, the spatial autocorrelation function normalized by its respective integral length-scale essentially collapses onto a single curve, as shown in Fig. 21(b). The collapse is less efficient at large displacements, which can be attributed mostly to optical aberration.

Additional statistical descriptions of turbulence at two independent points in the flow-field include various cross-spectra. The cross-spectrum, $S_{OH}(r,\omega)$, between two time series is defined as the Fourier transform of their space-time correlation (Priestly, 1981), as given by

$$S_{OH}(r,\omega) = \Im(f_{st}(r,\tau)).$$
(13)

Since the space-time correlation is usually not symmetric, the cross-spectrum is complex, i.e.,

$$S_{OH}(r,\omega) = Co_{OH}(\omega) - iQu_{OH}(\omega),$$
(14)

20

where the real part, $Co(\omega)$, is called the co-spectrum and the imaginary part, $Qu(\omega)$, is labeled the quadrature spectrum. As for the PSD, the co- and quadrature spectrum at any frequency, ω, represents the cross-covariance for the frequency components of the two time series at the same frequency, ω, where the co-spectrum corresponds to "in-phase" components and the quadrature spectrum corresponds to "out-of-phase" components. The OH cross-spectra at the four peak [OH] locations have similar shapes; thus, only one of them is presented in Fig. 21. The cross-spectra of the two-point time series taken at different displacements look very similar. The in-phase components are more correlated at frequencies less than 100 Hz while the out-of-phase components are generally uncorrelated over the whole frequency range, but with large fluctuations in the frequency range of 10-1000 Hz. The implications arising from such cross-spectra clearly require further investigation with respect to turbulent jet flames.

Refinement of Two-Point PITLIF

Optical aberrations were found to have significant effects on our previous two-point statistics (Zhang *et al.*, 2005). In essence, aberrations occur when either probe volume deviates from the optical axis of the collection system. Furthermore, at large displacement distances, partially overlap arises between probe volumes. This overlap creates artificial coherence between signals from the two probe volumes, which is exhibited as a secondary peak in the spatial autocorrelation function, as shown in Fig. 20. To address this problem, we designed a new lens system using ZEMAX software, which eventually produced a blur-spot of less than 100 μm at object positions up to 7 mm away from the optical axis. As shown in Fig. 22, the current optical system is composed of a custom-made aspherical lens (L1), a 4-inch diameter UV beamsplitter (BS) and two pairs of plano-convex and meniscus lenses (L2 and L3; L4 and L5). The new setup has a magnification ratio of 1.19 and a working f-number of 2.8.

To demonstrate the effectiveness of this revised setup, two-point data were taken at the same position (peak [OH] at $x/D = 20$) within the same flame used by Zhang *et al.* (2005). The derived spatial autocorrelation function shown in Fig. 23 has an approximately exponential decay without a secondary peak, as expected from the typical statistics of a turbulent field (Pope, 2000). A similar improvement is also observed in the space-time correlation, as shown in Fig. 24. Ongoing work is applying the new two-point technique to several standard non-premixed turbulent flames (DLR-A and DLR-B) and also to the sequence of partially premixed flames previously investigated by Raguraman (2005).
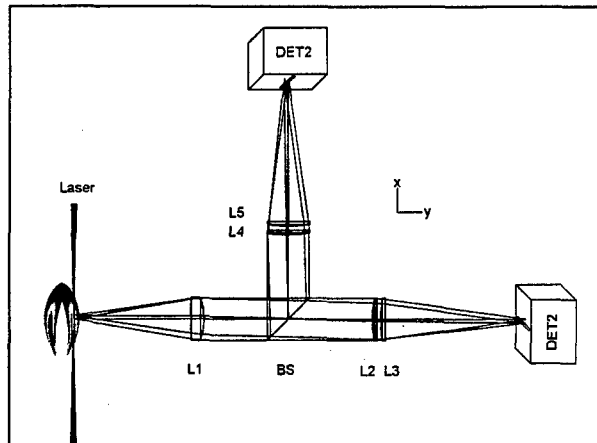

Figure 22. Detection optics for improved two-point PITLIF system. L, lens; BS, beam splitter; DET, detector assembly (monochromator and PMT). Red and blue rays identify signals from separate probe volumes.
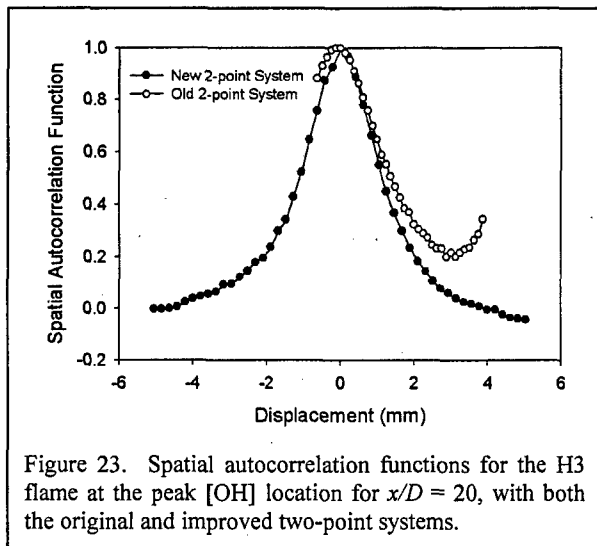

Figure 23. Spatial autocorrelation functions for the H3 flame at the peak [OH] location for $x/D = 20$, with both the original and improved two-point systems.

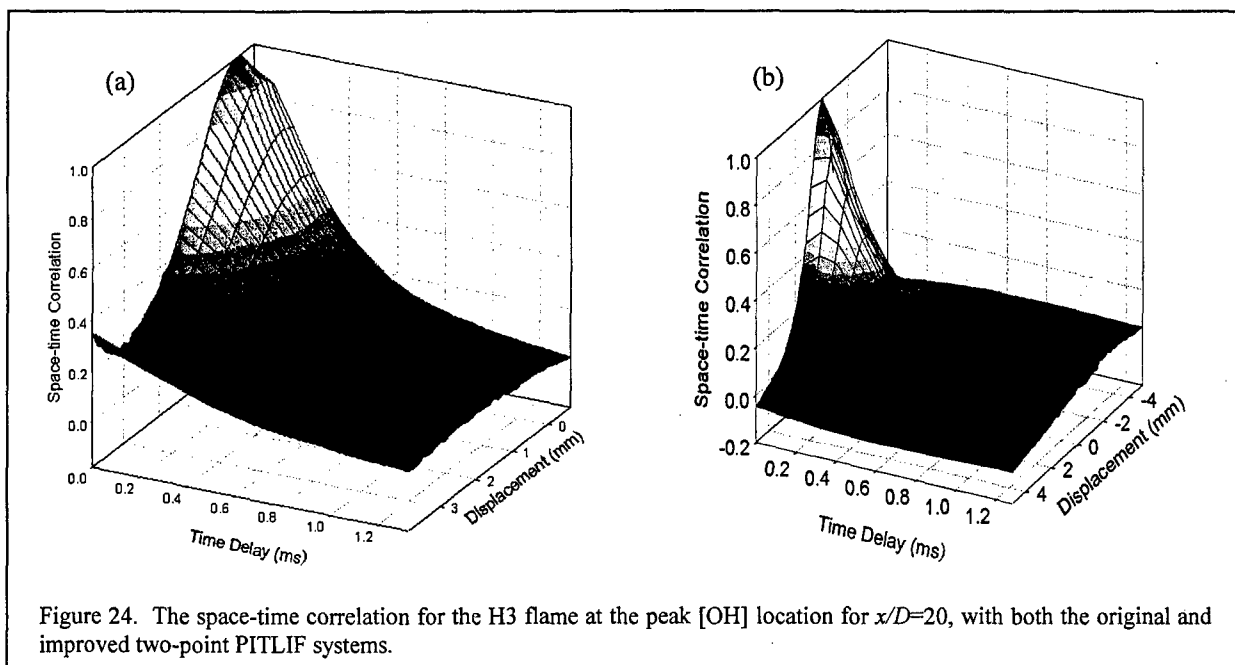## 4. Conclusions

Hydroxyl measurements in various non-premixed and partially premixed turbulent flames using PITLIF clearly demonstrates our capability for monitoring minor-species fluctuations at rates sufficiently

Figure 24. The space-time correlation for the H3 flame at the peak [OH] location for x/D=20, with both the original and improved two-point PITLIF systems.

rapid to permit the study of transient events in practical combustion environments. This information can be used to examine the accuracy of turbulence models, which purport to treat these flames, and to study the frequency content of turbulent fluctuations for minor species as compared to that of other scalars in the flow field. The major conclusions stemming from our recent PITLIF work can be summarized as follows:

1. Simultaneous fluorescence and lifetime measurements can now be made with a precision better than 10% at sampling rates beyond 10 kHz. Hence, time-series measurements can be obtained with sufficient temporal and spatial resolution to permit detailed, quantitative investigations of related autocorrelation functions, power spectral densities (PSDs) and integral time-scales.

2. Autocorrelation functions and PSDs for hydroxyl and total number density undergo a remarkable collapse for turbulent non-premixed and partially premixed flames when normalized by their local integral time-scales. In general, the ratio of number density to hydroxyl time-scale in both non-premixed and partially premixed flames is about 2-4. However, this ratio changes with radial location much more significantly in partially premixed flames than in non-premixed flames owing to the influence of partial premixing on the width of the OH layer.

3. One-dimensional stochastic and LES simulations based on the laminar flamelet model capture effectively time-scale variations for both hydroxyl and total number density in turbulent jet flames. In other words, independent measurements and simulations of these two time-scales are self-consistent, implying a single value of the underlying fluctuation rate in mixture fraction.

4. A two-point version of the PITLIF technique has been developed which is capable of determining spatial autocorrelation functions, integral length-scales and space-time correlations in turbulent flames. Current work is applying two-point PITLIF to standard non-premixed and partially premixed flames in the turbulent jet configuration.

In summary, AFOSR support during the past three years has provided quantitative data on integral time-scales for hydroxyl and total number density in non-premixed and partially premixed flames, including a new method for determining similar time-scales for the mixture fraction, which is a very challenging but important research goal. Stochastic modeling has thus far relied on mixture-fraction statistics from Raman scattering measurements as inputs owing to the heuristic nature of the simulations. PITLIF data is currently being shared with international colleagues so as to assess LES models for turbulent

combustion. Therefore, the advent of PITLIF has clearly presented new opportunities for understanding more completely the influence of heat release and velocity fluctuations on radical species in both turbulent non-premixed and partially premixed flames. Unfortunately, related spatial statistics are currently nonexistent for such flames; this situation is problematic given that interactions between turbulence and chemistry or between acoustics and heat transfer in partially premixed flames are undoubtedly of considerable importance for practical gas-turbine combustors and related thrust augmentors.

5. Personnel and Significant Collaborations

Professors Normand M. Laurendeau, Galen B. King, and Michael W. Renfro have been the co-principal investigators for this research program. Mr. Janak Raguraman and Mr. Krishna Kumar Venkatesan were M.S. students working on the project at Purdue University. Mr. Jiayao Zhang is a current Ph.D. student and Mr. Matthew Gluesenkamp is a current M.S. student at Purdue University. Ms. Yonghong Wang was an M.S. student working on the project at the University of Connecticut.

During the past three years, a collaborative PITLIF program has been established between our group at Purdue and the Air Force Research Laboratory (AFRL). The lead AFRL investigator is Dr. James Gord; other participating AFRL researchers include Dr. Sukesh Roy and Dr. Terry Meyer. Following an initial meeting at AFRL in June, 2002, we hosted a two-day visit by AFRL personnel at Purdue University in May, 2003. On the basis of these meetings, we agreed that an advanced PITLIF facility would be designed and built at AFRL under the direction of Prof. Galen King, who subsequently spent three 12-week periods at Wright Patterson Air Force Base in the summers of 2003, 2004 and 2005. Support came from Summer Faculty Fellowships via the National research Council (NRC) for the first two summers and via the American Society of Engineering Education (ASEE) for the third summer.

The main activity the first summer was construction and validation of the advanced PITLIF facility. The new instrument combines several improvements, owing to more modern components as compared to the original instrument built at Purdue in 1995-97. These improvements include a factor of eight longer temporal record (65,000 vs. 8,000 data points), a halving of the double-pulse resolution (3.3 vs. 6.5 ns.), and an enhanced capability for synchronization with other parts of the experiment.

During the second year, PITLIF measurements were combined with coordinated acetone and OH PLIF images of vortex structures formed in a counter-flow Rolon burner in which non-premixed vortices were generated using electromechanical actuators. The PITLIF technique was used to determine for the first time the temporal history of such vortex structures. In addition, PITLIF measurements of OH fluorescence signals enabled corrections for collisional quenching using known flames, thus giving PLIF-based number densities of OH within these vortex structures.

The major accomplishment from the third summer was the development of a new PITLIF-based thermometric method built on laser Rayleigh scattering (LRS). This diagnostic technique utilizes the residual second harmonic (~460 nm) remaining after the fundamental (919.5 nm) and second harmonic are mixed to produce the tripled frequency (306.5 nm) used to measure OH ($R_1(11)$). The LRS technique was applied to the same Rolon burner previously used for PITLIF measurements. Our intention is to employ this method for validation of LES-based combustion models both at AFRL and Purdue University.

6. Related Publications and Presentations

6.1 Refereed Journals

Zhang, J., Venkatesan, K.K., King, G.B., Laurendeau, N.M., and Renfro, M.W. (2005). Two-point time-series measurements of minor-species concentrations in a turbulent nonpremixed flame. *Optics Letters* **30**, 3144-3146.

Renfro, M.W., Chaturvedy, A., King, G. B., Laurendeau, N. M., Kempf, A., Dreizler, A., and Janicka, J. (2004). Comparison of OH time-series measurements and large-eddy simulations in hydrogen jet flames. *Combustion and Flame* **139**, 142-151.

Guttenfelder, W.A., King, G.B., Gore, J.P., Laurendeau, N.M. and Renfro, M.W. (2003). Hydroxyl time-series measurements and simulations for turbulent premixed jet flames in the thickened preheat regime. *Combustion and Flame* **135**, 381-403.

Renfro, M. W., Venkatesan, K. K., and Laurendeau, N. M. (2002). Cross-sections for CH quenching by N_2 and H_2O from 1740 to 2160 K. *Proc. Combust. Inst.* **29**, 2695-2702.

Renfro, M. W., Gore, J. P., and Laurendeau, N. M. (2002). Scalar time-series simulations for turbulent nonpremixed flames. *Combustion and Flame* **129**, 120-135.

6.2 Conference Proceedings and Presentations

Zhang, J., Venkatesan, K.K., King, G.B., Laurendeau, N.M., and Renfro, M.W. (2005). Two-point OH time-series measurements in a non-premixed turbulent jet flame. Proceedings of the Joint Meeting of the U.S. Sections of the Combustion Institute, Philadelphia, Pennsylvania.

Wang, Y., Renfro, M.W., Venkatesan, K.K., King, G.B., and Laurendeau, N.M. (2005). Bispectral analysis of scalar time series in turbulent flames. Proceedings of the Joint Meeting of the U.S. Sections of the Combustion Institute, Philadelphia, Pennsylvania.

Raguraman, J., King, G.B., Laurendeau, N.M. and Renfro, M.W. (2004). Hydroxyl and Rayleigh scattering time-series measurements in turbulent non-premixed $H_2/CH_4/N_2$-air jet flames. Proceedings of the Spring Technical Meeting, Central States Section of the Combustion Institute, San Antonio, Texas.

Wang, Y., Renfro, M.W., Chaturvedy, A., King, G.B. and Laurendeau, N.M. (2003). Evaluation of OH time-series asymmetries in turbulent non-premixed jet flames. Proceedings of the Fall Technical Meeting, Eastern States Section of the Combustion Institute, University Park, Pennsylvania.

Chaturvedy, A., King, G. B., Laurendeau, N. M., Renfro, M. W., Kempf, A., Dreizler, A., Sadiki, A. and Janicka, J. (2003). Comparison of OH time-series measurements and large-eddy simulations in H_2 jet flames. Proceedings of Third Joint Meeting of the U.S. Sections, The Combustion Institute, Chicago, IL.

6.3 Conference Posters

Zhang, J., Venkatesan, K.K., King, G.B., Laurendeau, N.M., and Renfro, M.W. (2005). Two-point OH time-series measurements in a non-premixed turbulent jet flame. Gordon Research Conference on Laser Diagnostics in Combustion, Mount Holyoke, Massachusetts.

King, G.B., Meyer, T.R., and Gord, J.P. (2005). Time history of flame-front/vortex interactions in a counter-flow jet burner. Gordon Research Conference on Laser Diagnostics in Combustion, Mount Holyoke, Massachusetts.

Chaturvedy, A., King, G. B., Laurendeau, N. M., Renfro, M. W., Kempf, A., Dreizler, A., Sadiki, A. and Janicka, J. (2003). Comparison of OH time-series measurements and large-eddy simulations in H_2 jet flames. Gordon Research Conference on Laser Diagnostics in Combustion, Oxford, England.

7. References

Barlow, R.S., and Carter, C.D. (1994), *Combust. Flame* **97**, 261.

Bergmann, V., Meier, W., Wolff, D., Stricker, W. (1998), *Appl. Phys. B* **66**, 489.

Bowman, C.T., Hanson, R.K., Davidson, D.F., Gardiner Jr., W.C., Lissianski, V., Smith, G.P., Golden, D.M., Frenklach, M., Goldenburg, M., http://www.me.berkley.edu/gri_mech/ (1995).

Box, G. E. P., and Jenkins, G. M. (1976), *Time Series Analysis*, Holden-Day, San Francisco.

Clemens, N. T. and Paul, P. H. (1995), *Combust. Flame* **102**, 271.

Drake, M.C. and Pitz, R.W. (1985), *Exp. Fluids* **3**, 283.

Dreizler, A. (2001), Technische Universität Darmstadt, Personal Communication.

Guttenfelder, W.A., Renfro, M.W., King, G.B., Laurendeau, N.M. (2003), *Combust. Flame* **135,** 381.

Han, D. and Mungal, M. G. (2000), *Proc. Combust. Inst.* **28**, 261.

Kempf, A., Sadiki, A., and Janicka, J. (2002), *Proc. Combust. Inst.* **29**, 1979.

Kounalakis, M.E., Sivathanu, Y.R., Faeth, G.M. (1991), *J. Heat Trans.* **113**, 437.

Landahl, M.T., and Mollo-Christensen, E. (1994), *Turbulence and Random Processes in Fluid Mechanics*, Cambridge University Press, New York.

Laurendeau, N.M. (1988), *Prog. Energy Combust. Sci.* **14,** 147.

Lutz, A.E., Kee, R.J., Grcar, J.F. (1996), Sandia National Laboratory, SAND96-8243.

Meier, W., Barlow, R. S., Chen, Y.-L. and Chen, J.-Y. (2000), *Combust. Flame* **123**, 326.

Meier, W., Prucker, S., Cao, M.H., Stricker, W. (1996), *Combust. Sci. Tech.* **118**, 293.

Neuber, A., Krieger, G., Tacke, M., Hassel, E., Janicka, J. (1998), *Combust. Flame* **113**, 198.

Pack, S.D., Renfro, M.W., King, G.B., Laurendeau, N.M. (1998), *Combust. Sci. Tech.* **140**, 405.

Pfuderer, D.G., Neuber, A.A., Früchtel, G., Hassel, E.P., Janicka, J. (1996), *Combust. Flame* **106**, 301

Pope, S. (2000), *Turbulent Flows*, Cambridge University Press, Cambridge, UK.

Priestly, M.B. (1981), *Spectral Analysis and Time Series*, Academic Press, Orlando, FL.

Raguraman, J. (2005), M.S. Thesis, School of Mechanical Engineering, Purdue University.

Raguraman, J., King, G.B., Laurendeau, N.M., Renfro, M.W. (2004), Spring Meeting, Central States Section, The Combustion Institute, Austion, Texas.

Reisel, J.R., Carter, C.D., and Laurendeau, N.M. (1997), *Energy and Fuels* **11**, 1092.

Renfro, M.W., Pack, S.D., King, G.B., Laurendeau, N.M. (1999a), *Appl. Phys. B* **69**, 137.

Renfro, M.W., King, G.B., Laurendeau, N.M. (1999b), *Appl. Opt.* **38**, 4596.

Renfro, M.W., Gore, J.P., King, G.B., Laurendeau, N.M. (2000a), *AIAA J.* **38**, 1230.

Renfro, M.W., Guttenfelder, W.A., King, G.B., Laurendeau, N.M. (2000b), *Combust. Flame* **123**, 389.

Renfro., M.W., Gore, J.P., Laurendeau, N.M. (2002), *Combust. Flame* **129**, 120.

Renfro, M.W., Chaturvedy, A., King, G.B., Laurendeau, N.M., Kempf, A., Dreisler, A., Janicka, J. (2004), Combust. Flame **139**, 142.

Schneider, Ch., Dreizler, A., Janicka, J. (2003), *Combust. Flame* **135**, 185.

Smith, G.P., Golden, D.M., Frenklach, M., Moriarity, N.W., Eiteneer, B., Goldenberg, M., Bowman, C.T., Hanson, R.K., Song, S., Gardiner, W.C., Lissianski, V.V., and Qin, Z. (1999), GRI Mechanism version 3.0, http://www.me.berkeley.edu/gri_mech/.

Wang, G.H., Clemens, N.T., Varghese, P.L. (2004), *Proc. Combust. Inst.* **30**, 30.

Zhang, J., Venkatesan, K.K., King, G.B., Laurendeau, N.M. Renfro, M.W. (2005), *Optics Letters* **30**, 3144.